TABLE 1 PV antigens in RIG-I- and MDA5-deficient mice

Organ or tissue	No. of PV antigen-positive mice/no. of mice tested			
	RIG-I$^{+/-}$ MDA5$^{+/-}$	RIG-I$^{-/-}$ MDA5$^{+/-}$	RIG-I$^{+/-}$ MDA5$^{-/-}$	RIG-I$^{-/-}$ MDA5$^{-/-}$
Brain	4/4	3/3	4/4	4/4
Spinal cord	4/4	3/3	4/4	4/4
Heart	0/4	0/3	0/4	0/4
Lung	0/4	0/3	0/4	0/4
Liver	0/4	0/3	0/4	0/4
Kidney	0/4	0/3	0/4	0/4
Spleen	0/4	0/3	0/4	0/4
Pancreas	0/4	0/3	0/4	0/4
Intestine	0/4	0/3	0/4	0/4
Adipose tissue	0/4	0/3	0/4	0/4

mice in the ICR background after intravenous infection with PV at 10^3, 10^4, and 10^5 PFU (Fig. 5A, B, and C). The mortality rates of these mice did not differ significantly from each other. We observed that the mortality rates of RIG-I$^{+/-}$ MDA5$^{-/-}$ mice that were inoculated with 10^4 PFU of PV was slightly higher than the mice of other genotypes. However, significant differences were not observed in mice that were inoculated with the other doses. Similar experiments were performed using MDA5$^{-/-}$ and MDA5$^{+/-}$ mice in the B6 background (Fig. 5D, E, and F). We did not observe significant differences between the MDA5$^{-/-}$ and MDA5$^{+/-}$ mice. The mortality rate of MDA5$^{-/-}$ mice was slightly higher than that of MDA5$^{+/-}$ mice that were inoculated with 10^5 PFU of PV. However, the opposite trend was observed when mice

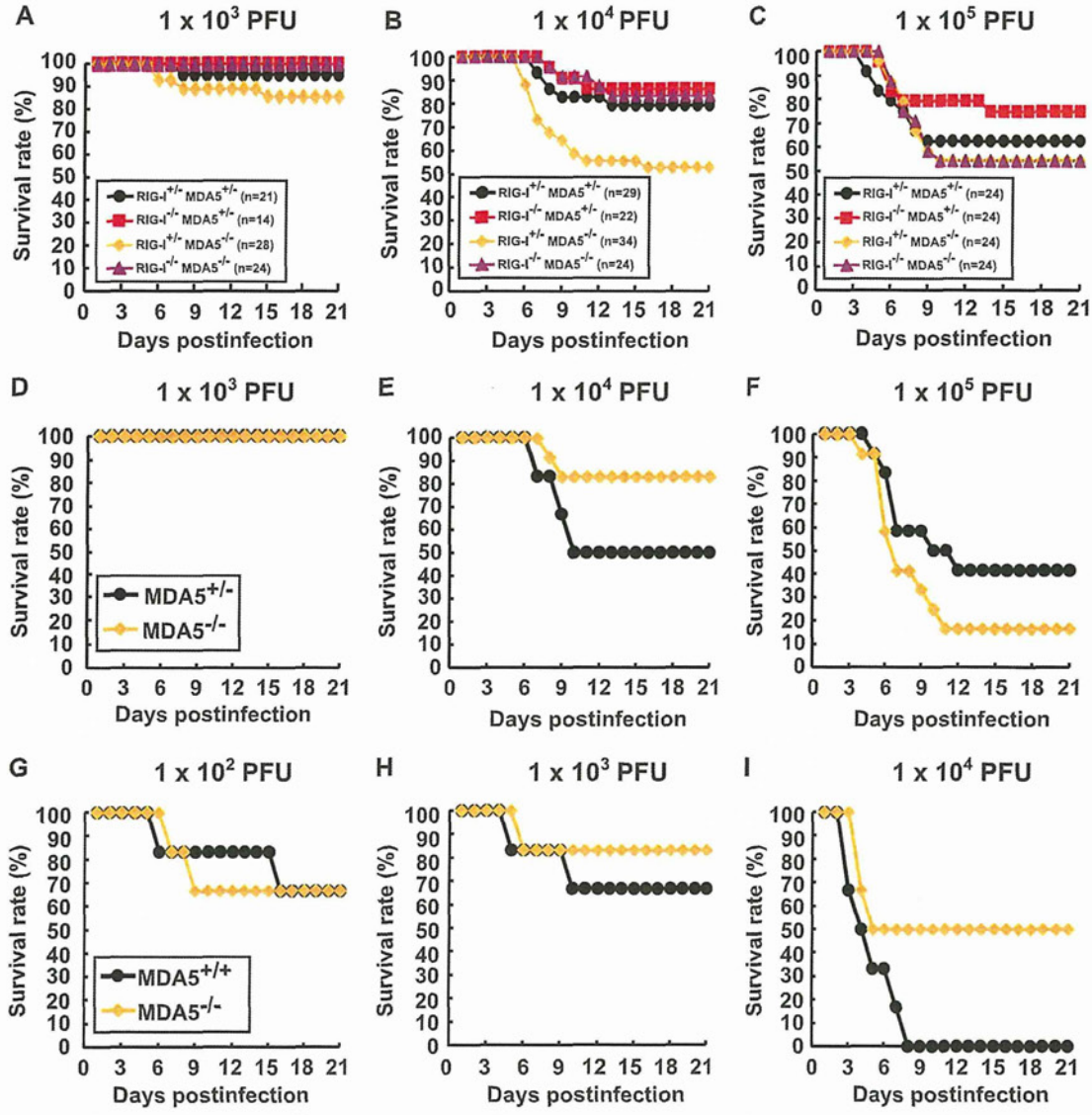

FIG 5 Mortality rates of RIG-I- and MDA5-deficient mice. Littermates of the genotypes indicated were obtained by mating RIGI-I$^{+/-}$ MDA5$^{+/-}$ and RIGI-I$^{-/-}$ MDA5$^{-/-}$ mice in the ICR background. The mice were infected intravenously with 10^3 (A), 10^4 (B), or 10^5 (C) PFU of PV. The results shown are the sums of several independent experiments. The total numbers of mice of the different genotypes that were used are boxed, and the doses used are shown at the top. Littermates of MDA5$^{+/-}$ and MDA5$^{-/-}$ mice were obtained in the B6 background. The mice (n = 12) were intravenously infected with 10^3 (D), 10^4 (E), or 10^5 (F) of PV. MDA5$^{+/+}$ and MDA5$^{-/-}$ mice (n = 6) were intracerebrally infected with 10^2 (G), 10^3 (H), or 10^4 (I) PFU of PV, respectively. We monitored the survival rates of the mice for 3 weeks after infection.

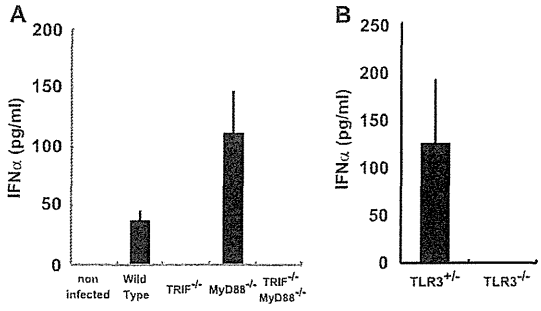

FIG 6 Production of serum IFN-α in TRIF-, MyD88-, and TLR3-deficient mice. Mice (n = 3 or 8) were intravenously infected with 10^7 PFU of PV. IFN-α levels of TRIF- and MyD88-deficient mice (A) and TLR3-deficient mice (B) at 12 hpi were compared. The experiments were repeated twice, and representative data are shown.

were inoculated with 10^4 PFU of PV. We suspect that the slight difference between the mortality rates of wild-type and MDA5$^{-/-}$ mice was in the range of experimental fluctuation, and thus, the disruption of MDA5 did not significantly influence the mortality rate. In order to determine if the same is true when mice are infected by other routes, we inoculated wild-type and MDA5$^{-/-}$ mice with PV intracerebrally and compared their mortality rates (Fig. 5G to I). Their mortality rates did not differ significantly. These results suggest that MDA5 does not make a great contribution to the protection of mice, at least after intracerebral and intravenous infections. Taken together, the MDA5-mediated response does not play a dominant role in IFN production, ISG induction, or inhibition of PV replication *in vivo*, unlike the MDA5-mediated effects on EMCV infection.

IFN response in TRIF- and MyD88-deficient mice. Because the experiments with MDA5-deficient mice suggested the existence of other protective mechanisms in PV infection, we investigated the role of TLRs using TRIF- and MyD88-deficient mice. PVR-tg mice were mated with TRIF$^{-/-}$ and/or MyD88$^{-/-}$ mice in the B6 background. Serum IFN-α of mice infected with 10^7 PFU of PV was measured using ELISA at 12 hpi (Fig. 6A). Interestingly, serum IFN production in response to PV infection was abrogated in TRIF$^{-/-}$ mice. Because TRIF acts as an adaptor for TLR3 and TLR4, we tested whether the same phenomenon occurs in TLR3$^{-/-}$ mice. Serum IFN induction was not observed in TLR3-deficient mice (Fig. 6B). These results suggest that the TLR3-mediated pathway is essential for IFN production in response to PV infection.

We next assessed the induction of mRNAs for OAS1a (Fig. 7A) and IRF-7 (Fig. 7B) in various organs using real-time RT-PCR. The induction of OAS1a and IRF-7 was observed in all mice. Although serum IFN production was abrogated in TRIF$^{-/-}$ mice and TRIF$^{-/-}$ MyD88$^{-/-}$ mice (Fig. 6), a significant level of ISG mRNA was induced. However, the induction levels were slightly lower than those in wild-type mice in some cases. The results suggest that the TRIF-mediated pathway contributes to ISG expression mainly through the induction of serum IFNs in response to PV infection and that some other mechanisms may also contribute to ISG expression.

PV replication in nonneural tissues and mortality rates of TRIF- and MyD88-deficient mice. The brain, spinal cord, liver, spleen, and kidney of paralyzed mice were recovered, and viral titers were determined (Fig. 8). PV was recovered from the CNS of TRIF$^{-/-}$, MyD88$^{-/-}$, and TLR3$^{-/-}$ mice, and the titers were not different from those of wild-type mice. However, the viral titers of the liver, spleen, and kidney of TRIF$^{-/-}$ and TLR3$^{-/-}$ mice were significantly higher than those of wild-type mice but lower than those of IFNAR1$^{-/-}$ mice. We then examined the virus replication kinetics in TRIF$^{-/-}$ mice (Fig. 8B). The viral load in the CNS increased in TRIF$^{-/-}$ mice similarly to that in other mice. In accordance to the absence of serum IFN (Fig. 2), the viral loads in the liver, spleen, and kidney of TRIF$^{-/-}$ mice increased, while the viral loads in these organs of wild-type mice decreased. PV antigens were detected in the CNS of all of the knockout mice. In addition, PV antigens were detected in the adipose tissue, pancreas, and kidney of several TRIF$^{-/-}$ and MyD88$^{-/-}$ mice (Table 2). These results suggest that these tissues support viral multiplication in these knockout mice and that the TLR-mediated signaling pathways contribute to the regulation of PV replication in nonneural tissues.

The mortality rates of TRIF$^{-/-}$, MyD88$^{-/-}$, and TLR3$^{-/-}$

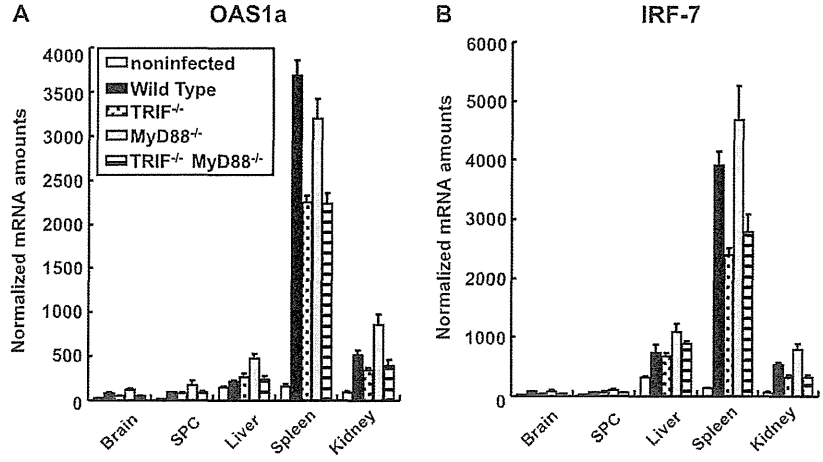

FIG 7 ISG induction in TRIF- and MyD88-deficient mice. Mice (n = 4) were intravenously infected with 10^7 PFU of PV. At 12 hpi, RNA was isolated from the indicated tissues of the infected mice and OAS1a (A) and IRF-7 (B) mRNA levels were determined by quantitative real-time PCR. The experiments were repeated twice, and representative data are shown. SPC, spinal cord.

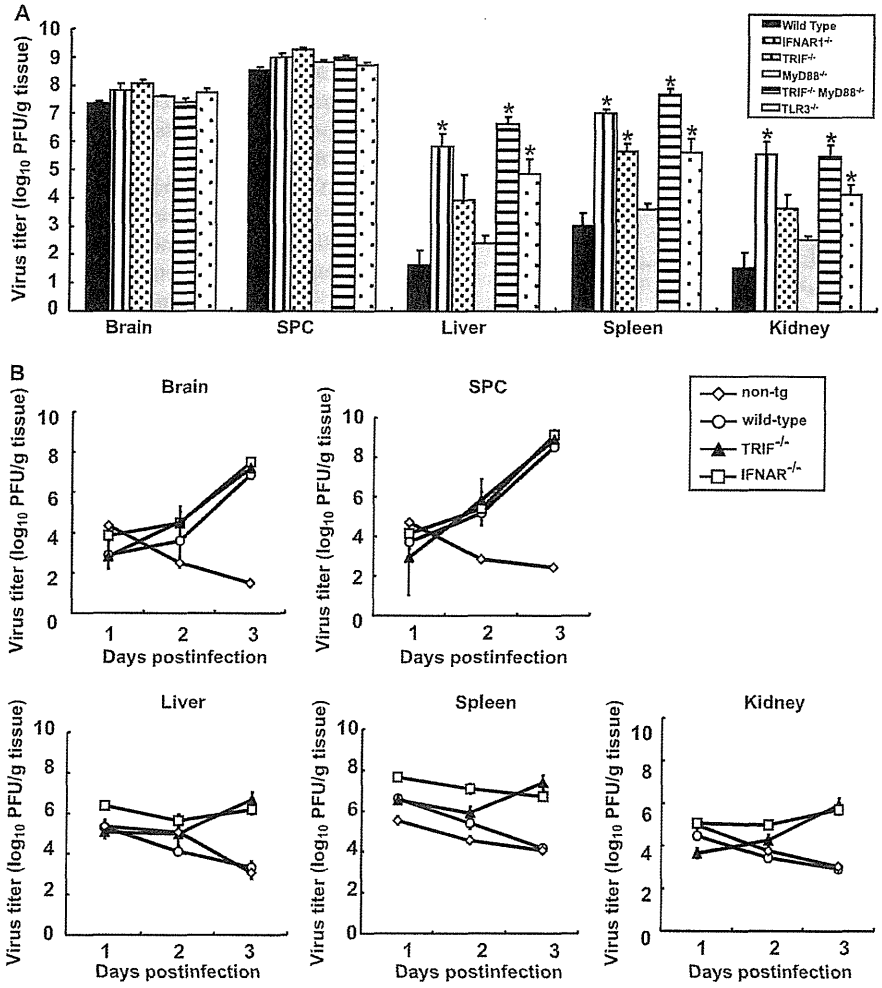

FIG 8 (A) PV replication in TRIF- and MyD88-deficient mice. Wild-type ($n = 4$), TRIF$^{-/-}$ ($n = 4$), MyD88$^{-/-}$ ($n = 6$), TRIF$^{-/-}$ MyD88$^{-/-}$ ($n = 4$), TLR3$^{-/-}$ ($n = 5$), and IFNAR1$^{-/-}$ ($n = 4$) mice were intravenously infected with 10^7 PFU of PV. The infected mice were paralyzed or dead at 3 to 5 days postinfection. The indicated tissues were collected, and viral titers were determined using a plaque assay (*, $P < 0.01$ by t test compared to wild-type mice). (B) PV replication kinetics in TRIF-deficient mice. Nontransgenic mice, wild-type mice, TRIF$^{-/-}$ mice, and IFNAR1$^{-/-}$ mice ($n = 3$) were infected as described above. Tissues were collected daily, and viral titers were determined. The results for nontransgenic (non-tg) mice, wild-type mice, and IFNAR1$^{-/-}$ mice are the same as those in Fig. 4B. SPC, spinal cord.

TABLE 2 PV antigens in TRIF- and MyD88-deficient mice

Organ or tissue	No. of PV antigen-positive mice/no. of mice tested			
	Wild type	TRIF$^{-/-}$	MyD88$^{-/-}$	TRIF$^{-/-}$ MyD88$^{-/-}$
Brain	6/6	8/8	9/9	6/6
Spinal cord	6/6	8/8	9/9	6/6
Heart	0/6	0/8	0/8	0/6
Lung	0/6	0/8	0/8	0/6
Liver	0/6	0/8	0/9	0/6
Kidney	0/6	0/8	2/9	0/5
Spleen	0/6	0/8	0/9	0/6
Pancreas	2/6	0/8	7/9	4/6
Intestine	0/6	0/8	0/9	0/6
Adipose tissue	0/6	2/8	2/9	3/6

mice were compared (Fig. 9). Approximately 25% of the TRIF$^{-/-}$ mice died after infection with 10^2 PFU of PV, and almost all of the mice died after infection with more than 10^3 PFU of PV (Fig. 9A). Approximately 20% and 60% of the MyD88$^{-/-}$ mice died after infection with 10^3 and 10^4 PFU of PV, respectively (Fig. 9B and C). TRIF$^{-/-}$ MyD88$^{-/-}$ mice were the most susceptible. In total, 70% of the mice died after infection with 10^2 PFU of PV (Fig. 9A). The mortality rate of TRIF$^{-/-}$ MyD88$^{-/-}$ mice was very close to that of IFNAR1$^{-/-}$ mice (19). The mortality rate of TLR3$^{-/-}$ mice was similar to that of TRIF$^{-/-}$ mice (Fig. 9D, E, and F). These results suggest that the TRIF-mediated and MyD88-mediated antiviral responses contribute to the host's defense against PV infection and that the TLR3-TRIF-mediated response has the most dominant effect.

DISCUSSION

Each virus infects different cell types and has a characteristic mode of replication. In mammalian hosts, several viral RNA sensors,

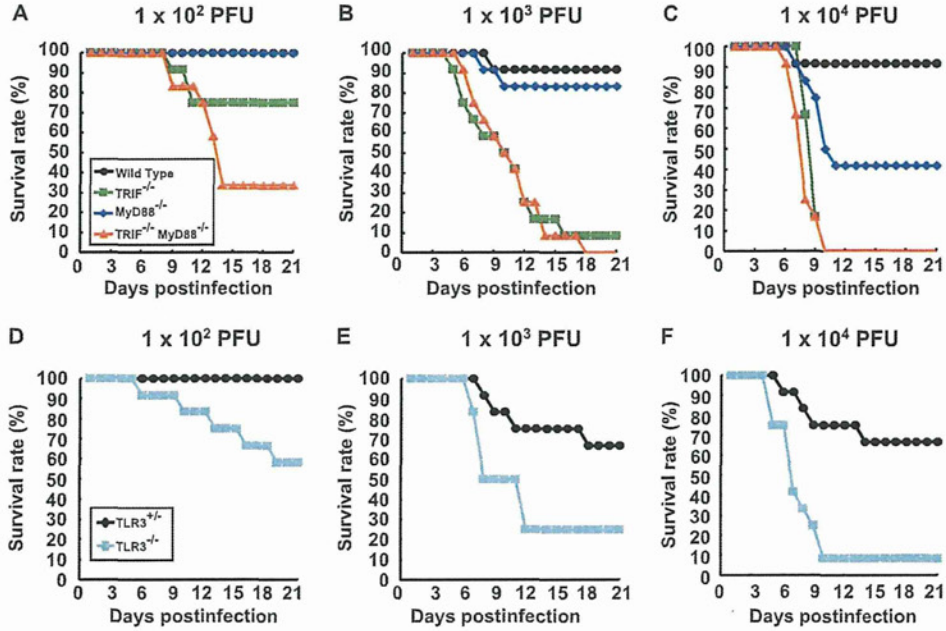

FIG 9 Mortality rates of TRIF-, MyD88-, and TLR3-deficient mice. (A) Wild-type, TRIF$^{-/-}$, MyD88$^{-/-}$, and TRIF$^{-/-}$ MyD88$^{-/-}$ mice (n = 12) were intravenously inoculated with the indicated doses of PV. (B) Littermates of TLR3$^{+/-}$ and TLR3$^{-/-}$ mice (n = 12) were used.

which are expressed in different cell types and recognize different molecular patterns, have evolved to counteract a variety of viruses. In the present study, we demonstrated that the MDA5-, TRIF-, and MyD88-mediated pathways contribute to the recognition of PV infection and that the TLR3-TRIF-mediated pathway plays the most important role in the antiviral response. Since all of the phenotypes shown after PV infection in the TRIF$^{-/-}$ mice and TLR3$^{-/-}$ mice are very similar to each other, we think that the contribution of the TLR3-mediated response is dominant and that of the TLR4-mediated response is negligible.

Previous reports have revealed that IFN is produced efficiently in EMCV-infected fibroblasts in an MDA5-dependent manner and that MDA5 contributes to the induction of serum IFNs and the protection of mice against EMCV (10, 23). Because EMCV belongs to the family *Picornaviridae*, we hypothesized that MDA5 also contributes to IFN induction in response to PV infection. However, the MDA5-dependent pathway did not play a dominant role in the defense against PV infection. Therefore, we speculate that PV uses mechanisms different from those of EMCV to strongly suppress IFN production *in vivo*. Indeed, IFN production in cultured cells in response to PV infection was observed only when the cells were pretreated with a low dose of IFNs. In addition, the amount of IFN produced was much lower than that produced in response to EMCV infection (Fig. 1). This result suggests that IFN induction in infected cells is suppressed and that this PV-mediated effect may be stronger than that of EMCV. Translational shutoff may be one of the reasons for this difference. PV 3A protein causes a change in membrane trafficking that prevents protein secretion and may also contribute to the suppression of IFN production (6). Caspase-dependent cleavage of MDA5 (3) and IPS-1 (39) in PV-infected cells has been reported. Through these possible mechanisms, PV may induce the suppression of IFN production in mice *in vivo*, and the MDA5-mediated pathway does not play an essential role in the host response, unlike in EMCV infection. PV and EMCV seemed to use different strategies to counteract the host innate immune system, even though PV and EMCV belong to the same family. Thus, TLR3 became the sensor that functions most effectively for PV as a result of PV evolution. Although the TLR3-TRIF-mediated pathway plays a dominant role, the fact that significant ISG induction was observed in PV-infected TRIF$^{-/-}$ and TRIF$^{-/-}$ MyD88$^{-/-}$ mice (Fig. 7) suggested that other mechanisms also operate in combination with this pathway.

The viral loads in the nonneural tissues of TLR3- and TRIF-deficient mice were much higher than those in wild-type mice, whereas the viral loads in the CNS were not significantly different in paralyzed mice (Fig. 8). These results suggest that the TLR3-TRIF-mediated pathway inhibits viral replication mainly before viral invasion of the CNS rather than after invasion and that this response plays an important role in preventing the viral invasion of the CNS. In the CNS, replication of PV was not effectively inhibited, even in wild-type mice. This result is consistent with our previous results obtained using IFNAR1$^{-/-}$ mice and suggests that the antivirus response in the CNS is different from that in nonneural tissues upon PV infection (19). The cell tropism of PV may influence the efficiency of the immune response. For example, if PVR is expressed in TLR3-expressing cells, then PV replication would be detected immediately after infection. Alternatively, if PV infection *in vivo* occurs in the vicinity of TLR3-expressing immune cells such as DCs and macrophages, PV-infected cells may readily be captured by TLR3-expressing cells, thereby facilitating efficient cross-priming (27, 44) of PV RNA. PV infects neurons almost exclusively and not other cell types in the CNS. If neurons do not have the ability to induce a strong TLR3-mediated antiviral response upon PV infection, the CNS may be more defective in the innate immune response than nonneural tissues are. This may be one of the reasons why PV replicates preferentially in the CNS. Further studies on PV pathogenesis related to the innate

immune response will make a great contribution to elucidating the mechanisms of PV tissue tropism.

TLR3 recognizes dsRNA. However, the protective role of TLR3 in the response to many RNA viral infections is not clear (9, 29, 43). A previous study has demonstrated that WNV, which is an encephalitis virus belonging to the family *Flaviviridae*, causes more severe encephalitis in mice with intact TLR3 than in TLR3$^{-/-}$ mice. Peripheral WNV infection leads to a breakdown of the blood-brain barrier (BBB) and enhances brain infection in wild-type mice but not in TLR3$^{-/-}$ mice (50). In contrast, a protective role of the TLR3-mediated pathway in PV infection was clearly demonstrated in the present study. PV enters the CNS directly across the BBB via a PVR-independent mechanism (52) and from the neuromuscular junction via retrograde axonal transport (31–33). Because PV originally possesses two entry pathways into the CNS, the generation of a new entry pathway, even if it did occur, might not increase its deteriorative effect.

Interestingly, protective roles of the TLR3-mediated pathway have been reported for group B coxsackievirus (30, 41, 42), human rhinovirus (49), and EMCV (11) infections. Riad et al. (41) demonstrated that TRIF$^{-/-}$ mice showed severe myocarditis after CVB3 infection and IFN-β treatment improved virus control and reduced cardiac inflammation. Richer et al. (42) reported that TLR3$^{-/-}$ mice produced reduced proinflammatory mediators and were unable to control CVB4 replication at the early stages of infection, resulting in severe cardiac damage. They also showed that adoptive transfer of wild-type macrophages into TLR3$^{-/-}$ mice challenged with CVB4 resulted in greater survival, suggesting the importance of the TLR3-mediated pathway in the macrophage. Negishi et al. (30) reported that TLR3$^{-/-}$ mice showed vulnerability to CVB3 and that TLR3 signaling is linked to the activation of the type II IFN system. Since CVB3 does not induce robust type I IFNs, they suggested that the TLR3 type II IFN pathway serves as an "ace in the hole" in infections with such viruses. PV is similar to CVB3 because type I IFN production is low. However, in our preliminary experiments on PV infection in IFN-$\gamma^{-/-}$ PVR-tg mice, type II IFN did not make a significant contribution to the pathogenesis of PV. Taken together, these results suggest a critical role for the TLR3-mediated pathway, but the precise mechanisms leading to host protection are still controversial and the downstream events of TLR3 signaling after picornavirus infection remain to be elucidated.

Because the above-mentioned viruses are picornaviruses, picornavirus RNA may be easily detected by TLR3. There may be a common RNA structure in the genome or in the replication intermediates of these viruses that is detected by TLR3. Alternatively, picornaviral RNA may replicate in a compartment in which TLR3 can easily access the replicating dsRNA. To investigate these hypotheses, identification of the cells responsible for IFN production is an important step. Oshiumi et al. demonstrated that splenic CD8α^+ CD11c$^+$ cells, bone marrow-derived macrophages, and DCs are able to elicit IFN in response to PV infection (35). Further studies using this virus-cell system will elucidate the molecular recognition pattern in the PV genome, the precise mechanism of PV RNA recognition in TLR3-expressing cells, and the roles of these cells in the prevention of PV dissemination in the body.

ACKNOWLEDGMENTS

We thank Takashi Fujita, Mitsutoshi Yoneyama, Hiroki Kato, Masahiro Yamamoto, Satoshi Uematsu, Seiya Yamayoshi, Akira Ainai, Hideki Hasegawa, and Takashi Kawanishi for helpful discussions and technical assistance.

This work was supported, in part, by Grants-in-Aid from the Ministry of Education, Culture, Sports, Science and Technology, Japan (Grants-in-Aid for Scientific Research on Priority Areas no. 21022053), and Grants-in-Aid for Research on Emerging and Re-emerging Infectious Diseases from the Ministry of Health, Labor and Welfare, Japan.

REFERENCES

1. **Akira S, Uematsu S, Takeuchi O.** 2006. Pathogen recognition and innate immunity. Cell **124**:783–801.
2. **Alexopoulou L, Holt AC, Medzhitov R, Flavell RA.** 2001. Recognition of double-stranded RNA and activation of NF-kappaB by Toll-like receptor 3. Nature **413**:732–738.
3. **Barral PM, et al.** 2007. MDA-5 is cleaved in poliovirus-infected cells. J. Virol. **81**:3677–3684.
4. **Bodian D.** 1959. Poliomyelitis: pathogenesis and histopathology, p 479–518. *In*Rivers TM, Horsfall FL, Jr (ed), Viral and rickettsial infections of man, vol 3. J. B. Lippincott, Philadelphia, PA.
5. **Cella M, et al.** 1999. Plasmacytoid monocytes migrate to inflamed lymph nodes and produce large amounts of type I interferon. Nat. Med. **5**:919–923.
6. **Choe SS, Dodd DA, Kirkegaard K.** 2005. Inhibition of cellular protein secretion by picornaviral 3A proteins. Virology **337**:18–29.
7. **Colonna M, Trinchieri G, Liu YJ.** 2004. Plasmacytoid dendritic cells in immunity. Nat. Immunol. **5**:1219–1226.
8. **Diebold SS, Kaisho T, Hemmi H, Akira S, Reis e Sousa C.** 2004. Innate antiviral responses by means of TLR7-mediated recognition of single-stranded RNA. Science **303**:1529–1531.
9. **Edelmann KH, et al.** 2004. Does Toll-like receptor 3 play a biological role in virus infections? Virology **322**:231–238.
10. **Gitlin L, et al.** 2006. Essential role of mda-5 in type I IFN responses to polyriboinosinic:polyribocytidylic acid and encephalomyocarditis picornavirus. Proc. Natl. Acad. Sci. U. S. A. **103**:8459–8464.
11. **Hardarson HS, et al.** 2007. Toll-like receptor 3 is an essential component of the innate stress response in virus-induced cardiac injury. Am. J. Physiol. Heart Circ. Physiol. **292**:H251–H258.
12. **Hemmi H, et al.** 2002. Small anti-viral compounds activate immune cells via the TLR7 MyD88-dependent signaling pathway. Nat. Immunol. **3**:196–200.
13. **Hoebe K, et al.** 2003. Identification of Lps2 as a key transducer of MyD88-independent TIR signalling. Nature **424**:743–748.
14. **Holland JJ.** 1961. Receptor affinities as major determinants of enterovirus tissue tropisms in humans. Virology **15**:312–326.
15. **Holland JJ, Mc LL, Syverton JT.** 1959. Mammalian cell-virus relationship. III. Poliovirus production by non-primate cells exposed to poliovirus ribonucleic acid. Proc. Soc. Exp. Biol. Med. **100**:843–845.
16. **Holland JJ, McLaren LC, Syverton JT.** 1959. The mammalian cell-virus relationship. IV. Infection of naturally insusceptible cells with enterovirus ribonucleic acid. J. Exp. Med. **110**:65–80.
17. **Hornung V, et al.** 2006. 5′-Triphosphate RNA is the ligand for RIG-I. Science **314**:994–997.
18. **Hsiung GD, Black FL, Henderson JR.** 1964. Susceptibility of primates to viruses in relation to taxonomic classification, p 1–23. *In*Buettner-Jaenusch J (ed), Evolutionary and genetic biology of primates, vol 2. Academic Press, New York, NY.
19. **Ida-Hosonuma M, et al.** 2005. The alpha/beta interferon response controls tissue tropism and pathogenicity of poliovirus. J. Virol. **79**: 4460–4469.
20. **Ida-Hosonuma M, et al.** 2003. Host range of poliovirus is restricted to simians because of a rapid sequence change of the poliovirus receptor gene during evolution. Arch. Virol. **148**:29–44.
21. **Kato H, et al.** 2005. Cell type-specific involvement of RIG-I in antiviral response. Immunity **23**:19–28.
22. **Kato H, et al.** 2008. Length-dependent recognition of double-stranded ribonucleic acids by retinoic acid-inducible gene-I and melanoma differentiation-associated gene 5. J. Exp. Med. **205**:1601–1610.
23. **Kato H, et al.** 2006. Differential roles of MDA5 and RIG-I helicases in the recognition of RNA viruses. Nature **441**:101–105.
24. **Koike S, et al.** 1992. A second gene for the African green monkey poliovirus receptor that has no putative N-glycosylation site in the functional N-terminal immunoglobulin-like domain. J. Virol. **66**:7059–7066.

25. Koike S, Nomoto A. 2010. Poliomyelitis, p 339–351. *In*Ehrenfeld E, Domingo E, Roos RP (ed), The picornaviruses. ASM Press, Washington, DC.
26. Koike S, et al. 1991. Transgenic mice susceptible to poliovirus. Proc. Natl. Acad. Sci. U. S. A. 88:951–955.
27. Kramer M, et al. 2008. Phagocytosis of picornavirus-infected cells induces an RNA-dependent antiviral state in human dendritic cells. J. Virol. 82:2930–2937.
28. Matsumoto M, et al. 2003. Subcellular localization of Toll-like receptor 3 in human dendritic cells. J. Immunol. 171:3154–3162.
29. Matsumoto M, Oshiumi H, Seya T. 2011. Antiviral responses induced by the TLR3 pathway. Rev. Med. Virol. 21:67–77.
30. Negishi H, et al. 2008. A critical link between Toll-like receptor 3 and type II interferon signaling pathways in antiviral innate immunity. Proc. Natl. Acad. Sci. U. S. A. 105:20446–20451.
31. Ohka S, et al. 2004. Receptor (CD155)-dependent endocytosis of poliovirus and retrograde axonal transport of the endosome. J. Virol. 78: 7186–7198.
32. Ohka S, et al. 2009. Receptor-dependent and -independent axonal retrograde transport of poliovirus in motor neurons. J. Virol. 83:4995–5004.
33. Ohka S, Yang WX, Terada E, Iwasaki K, Nomoto A. 1998. Retrograde transport of intact poliovirus through the axon via the fast transport system. Virology 250:67–75.
34. Oshiumi H, Matsumoto M, Funami K, Akazawa T, Seya T. 2003. TICAM-1, an adaptor molecule that participates in Toll-like receptor 3-mediated interferon-beta induction. Nat. Immunol. 4:161–167.
35. Oshiumi H, et al. 12 October 2011, posting date. The TLR3-TICAM-1 pathway is mandatory for innate immune responses to poliovirus infection. J. Immunol. [Epub ahead of print.] doi:10.4049/jimmunol.1101503.
36. Pichlmair A, et al. 2006. RIG-I-mediated antiviral responses to single-stranded RNA bearing 5′-phosphates. Science 314:997–1001.
37. Pichlmair A, et al. 2009. Activation of MDA5 requires higher-order RNA structures generated during virus infection. J. Virol. 83:10761–10769.
38. Racaniello VR. 2007. Picornaviridae: the viruses and their replication, p 795–838. *In*Knipe DM, Howley PM (ed), Fields virology, 5th ed. Lippincott Williams & Wilkins, Philadelphia, PA.
39. Rebsamen M, Meylan E, Curran J, Tschopp J. 2008. The antiviral adaptor proteins Cardif and Trif are processed and inactivated by caspases. Cell Death Differ. 15:1804–1811.
40. Ren RB, Costantini F, Gorgacz EJ, Lee JJ, Racaniello VR. 1990. Transgenic mice expressing a human poliovirus receptor: a new model for poliomyelitis. Cell 63:353–362.
41. Riad A, et al. 2011. TRIF is a critical survival factor in viral cardiomyopathy. J. Immunol. 186:2561–2570.
42. Richer MJ, Lavallee DJ, Shanina I, Horwitz MS. 2009. Toll-like receptor 3 signaling on macrophages is required for survival following coxsackievirus B4 infection. PLoS One 4:e4127.
43. Schröder M, Bowie AG. 2005. TLR3 in antiviral immunity: key player or bystander? Trends Immunol. 26:462–468.
44. Schulz O, et al. 2005. Toll-like receptor 3 promotes cross-priming to virus-infected cells. Nature 433:887–892.
45. Shiroki K, et al. 1995. A new *cis*-acting element for RNA replication within the 5′ noncoding region of poliovirus type 1 RNA. J. Virol. 69: 6825–6832.
46. Takeuchi O, Akira S. 2009. Innate immunity to virus infection. Immunol. Rev. 227:75–86.
47. Takeuchi O, Akira S. 2008. MDA5/RIG-I and virus recognition. Curr. Opin. Immunol. 20:17–22.
48. Takeuchi O, Akira S. 2007. Recognition of viruses by innate immunity. Immunol. Rev. 220:214–224.
49. Wang Q, et al. 2009. Role of double-stranded RNA pattern recognition receptors in rhinovirus-induced airway epithelial cell responses. J. Immunol. 183:6989–6997.
50. Wang T, et al. 2004. Toll-like receptor 3 mediates West Nile virus entry into the brain causing lethal encephalitis. Nat. Med. 10:1366–1373.
51. Yamamoto M, et al. 2003. Role of adaptor TRIF in the MyD88-independent Toll-like receptor signaling pathway. Science 301:640–643.
52. Yang WX, et al. 1997. Efficient delivery of circulating poliovirus to the central nervous system independently of poliovirus receptor. Virology 229:421–428.
53. Yoneyama M, et al. 2004. The RNA helicase RIG-I has an essential function in double-stranded RNA-induced innate antiviral responses. Nat. Immunol. 5:730–737.
54. Yoshikawa T, et al. 2006. Role of the alpha/beta interferon response in the acquisition of susceptibility to poliovirus by kidney cells in culture. J. Virol. 80:4313–4325.
55. Yousefi S, Escobar MR, Gouldin CW. 1985. A practical cytopathic effect/dye-uptake interferon assay for routine use in the clinical laboratory. Am. J. Clin. Pathol. 83:735–740.

Toxicology Letters 214 (2012) 9–18

Contents lists available at SciVerse ScienceDirect

Toxicology Letters

journal homepage: www.elsevier.com/locate/toxlet

Chimeric mice with a humanized liver as an animal model of troglitazone-induced liver injury

Masakazu Kakuni[a], Mayu Morita[b], Kentaro Matsuo[b], Yumiko Katoh[a], Miki Nakajima[b], Chise Tateno[a], Tsuyoshi Yokoi[b,*]

[a] PhoenixBio Co., Ltd., Hiroshima 739-0046, Japan
[b] Division of Pharmaceutical Sciences, Faculty of Pharmaceutical Sciences, Kanazawa University, Kakuma-machi, Kanazawa 920-1192, Japan

HIGHLIGHTS

- Troglitazone (Tro) was withdrawn due to its association with severe liver injury.
- Orally administered Tro has never induced liver injury in experimental animals.
- The chimeric mice with a humanized liver reproduced Tro-induced liver injury.
- Possible factors that contribute to the Tro-induced liver injury were evaluated.
- This mouse model enables human hepatocytes to be examined in an *in vivo* environment.

ARTICLE INFO

Article history:
Received 11 April 2012
Received in revised form 31 July 2012
Accepted 2 August 2012
Available online xxx

Keywords:
Chimeric mouse with a humanized liver
Drug-induced liver injury (DILI)
Hepatotoxicity
Troglitazone
Glutathione

ABSTRACT

Troglitazone (Tro) is a thiazolidinedione antidiabetic drug that was withdrawn from the market due to its association with idiosyncratic severe liver injury. Tro has never induced liver injury in experimental animals *in vivo*. It was assumed that the species differences between human and experimental animals in the pharmaco- or toxicokinetics of Tro might be associated with these observations. In this study, we investigated whether a chimeric mouse with a humanized liver that we previously established, whose replacement index with human hepatocytes is up to 92% can reproduce Tro-induced liver injury. When the chimeric mice were orally administered Tro for 14 or 23 days (1000 mg/kg/day), serum alanine aminotransferase (ALT) was significantly increased by 2.1- and 3.6-fold, respectively. Co-administration of L-buthionine sulfoximine (10 mM in drinking water), an inhibitor of glutathione (GSH) synthesis, unexpectedly prevented the Tro-dependent increase of ALT, which suggests that the GSH scavenging pathway will not be involved in Tro-induced liver injury. To elucidate the mechanism of the onset of liver injury, hepatic GSH content, the level of oxidative stress markers and phase I and phase II drug metabolizing enzymes were determined. However, these factors were not associated with Tro-induced liver injury. An immune-mediated reaction may be associated with Tro-induced liver toxicity *in vivo*, because the chimeric mouse is derived from an immunodeficient SCID mouse. In conclusion, we successfully reproduced Tro-induced liver injury using chimeric mice with a humanized liver, which provides a new animal model for studying idiosyncratic drug-induced liver injury.

1. Introduction

Troglitazone (Tro) was the first thiazolidinedione used for treating of type II diabetes mellitus, but was withdrawn due to serious idiosyncratic liver injury. During the preclinical development of Tro, no study could predict the hepatotoxic effect of Tro in human (Watanabe et al., 1999). After the withdrawal of Tro from the market, numerous studies using animal models were performed to reproduce the hepatotoxicity of Tro, but almost all were unsuccessful (Bedoucha et al., 2001; Jia et al., 2000; Watanabe et al., 2000).

Ong et al. (2007) reported that the administration of Tro (30 mg/kg, *i.p.*) to heterozygous superoxide dismutase 2 (SOD2) knockout ($SOD2^{+/-}$) mice resulted in hepatocellular necrosis and increased serum alanine aminotransferase (ALT) levels, suggesting that SOD2, which is expressed mainly in the mitochondria, plays a crucial role in Tro-induced liver injury. However, other research group could not reproduce these results using the same

* Corresponding author at: Drug Metabolism and Toxicology, Faculty of Pharmaceutical Sciences, Kanazawa University, Kakuma-machi, Kanazawa 920-1192, Japan. Tel.: +81 76 234 4407; fax: +81 76 234 4407.
E-mail address: tyokoi@kenroku.kanazawa-u.ac.jp (T. Yokoi).

0378-4274/$ – see front matter © 2012 Elsevier Ireland Ltd. All rights reserved.
http://dx.doi.org/10.1016/j.toxlet.2012.08.001

heterozygous SOD2 knockout mice (Fujimoto et al., 2009). No further studies of *in vivo* animal models have been reported.

Because idiosyncratic liver injury is a human-specific toxic event, we surmised that previously established chimeric mice with a humanized liver (Tateno et al., 2004) might be useful as an animal model. In this study, we investigated whether Tro causes liver injury in a chimeric mouse with a humanized liver, which was derived from a urokinase-type plasminogen activator$^{+/+}$/severe combined immunodeficient transgenic (uPA$^{+/+}$/SCID mouse) mouse line. In this animal model, more than 75% of the mouse hepatocytes are replaced with human hepatocytes in which the human mRNAs and proteins expression levels and enzyme activities were evaluated (Katoh et al., 2004, 2005, 2007; Nishimura et al., 2005).

Tro undergoes metabolic activation by CYPs, in particular, the CYP3A4 isoform, to form reactive metabolites that bind covalently to proteins and nucleophiles, such as glutathione (GSH) and cysteine. Various reactive metabolites of Tro were identified as GSH conjugates (Tettey et al., 2001; Kassahun et al., 2001; He et al., 2004). The susceptibility of drugs metabolized to reactive intermediates is different between GSH-depleted animals and normal animals (T. Watanabe et al., 2003; Usui et al., 2011). Therefore, we expected that Tro would exhibit hepatotoxic effects under a GSH-depleted condition. L-Buthionine sulfoximine (BSO), a well-known inhibitor of GSH synthesis, was selected to investigate the relationship between the GSH conjugation ability and Tro-induced hepatotoxicity.

In the present study, we orally administered Tro for 14 or 23 days to chimeric mice with a humanized liver and reproduced liver injury. Subsequently, possible factors that were expected to contribute to the development of Tro-induced liver injury, such as drug-metabolizing enzymes, GSH, SOD2, and protein carbonyl contents, were evaluated.

2. Materials and methods

2.1. Chemicals

TRO was kindly provided by Daiichi Sankyo (Tokyo, Japan). L-Buthionine sulfoximine (BSO) and paclitaxel were purchased from Sigma (St. Louis, MO). ReverTra Ace was from Toyobo (Tokyo, Japan). Random hexamer, RNAiso, SYBR Premix Ex Taq, and ROX Reference Dye II were from Takara (Osaka, Japan). Recombinant human CYP2C8 and CYP3A4 expressed in baculovirus-infected insect cells and 6a-hydroxypaclitaxel were from BD Gentest (Woburn, MA). Dexamethasone and testosterone were from Wako Pure Chemical Industries (Osaka, Japan). 6b-Hydroxytestosterone was from Sekisui Medical (Tokyo, Japan). All primers were commercially synthesized at Hokkaido System Sciences (Sapporo, Japan). The polyclonal rabbit anti-human CYP2C8 antibody was from Nosan (Yokohama, Japan) and the polyclonal goat anti-CYP3A antibody (sc-30621) was from Santa Cruz Biotechnology (Santa Cruz, CA). All other chemicals were of analytical or the highest grade commercially available.

2.2. Generation of the chimeric mice with a humanized liver

The present study was conducted in accordance with the National Institutes of Health Guide for Animal Welfare of Japan, and the protocols were approved by the Institutional Animal Care and Use Committees of Kanazawa University (Kanazawa, Japan) and PhoenixBio Co., Ltd. (Hiroshima, Japan). The chimeric mice were generated by PhoenixBio. Briefly, commercially available cryopreserved human hepatocytes (5-year-old African-American male from BD Gentest) were transplanted into the spleens of uPA$^{+/+}$/SCID mice at approximately 3–4 weeks of age. At mice's age of 6–7 weeks, the monitoring of human albumin (h-Alb) concentration in blood was started and continued until the start of the study when the chimeric mice were 11–15 weeks old. Two microliters of blood was collected from tail vein of the mice once per week, and the concentrations of hAlb in the blood of the chimeric mice were determined by latex agglutination immunonephelometry to estimate the rate of replacement of mouse hepatocytes with human hepatocytes (RI: Replacement Index). The correlation between hAlb and the actual RI has been determined based on immunohistochemistry conducted with anti-human specific cytokeratin 8 and 18 antibodies (Tateno et al., 2004). The chimeric mice used in the present study were female, 11–15 weeks old, and exhibited concentrations of 8.0–14.9 mg/ml of hAlb or an RI of 75–92% at the start of the TRO administration (Table 1). The animals were housed in a controlled environment (temperature 23 ± 1 °C, humidity 57 ± 15%, and 12 h light/12 h dark cycle) in the institution's animal facility with *ad libitum* access to food and water.

2.3. Drug and/or BSO administration

The chimeric mice were orally administered Tro [250 mg/kg/10 ml, 500 mg/kg/ml or 1000 mg/kg/10 ml, suspended in 0.5% carboxymethylcellulose (CMC)] once daily for 14 (1000 mg/kg), 23 (1000 mg/kg) or 28 (250 and 500 mg/kg) days in a non-fasting condition, and 0.5% CMC was administered once daily as a control. BSO (10 mM) in sterilized tap water was also administered *via* drinking water alone or with Tro. Water bottle was changed twice a week during the BSO treatment. The dosing method was originally reported by T. Watanabe et al. (2003), in which 5–30 mM of BSO in drinking water had been confirmed to be stable for 15 days at 23 °C without light-shielded conditions. Pre-dosing blood samples were collected under isoflurane anesthesia to measure the initial serum ALT level. Twenty-four hours after the last Tro administration, the blood and livers were collected by exsanguination under isoflurane anesthesia. Serum ALT, aspartate aminotransferase (AST), bilirubin (total bilirubin: T-Bil, and direct bilirubin: D-Bil) and lactate dehydrogenase (LDH) levels were measured using FUJI DRI-CHEM (FUJIFILM, Tokyo, Japan). A portion of the liver was fixed in buffered neutral 10% formalin. The fixed samples were embedded in paraffin, sectioned at a thickness of 2 μm and stained with hematoxylin–eosin (H&E) for microscopic examination.

2.4. GSH level

Mouse livers were homogenized in ice-cold 5% sulfosalicylic acid using a glass homogenizer and centrifuged at 8000 × *g* at 4 °C for 10 min. The GSH concentration in the supernatant was measured as described previously (Tietze, 1969).

2.5. Glutathione S-transferase (GST) activity

GST activity was measured according to the method of Habig et al. (1974) with slight modifications. The incubation mixtures consisted of cytosol (0.1 ml) in 125 mM potassium phosphate buffer (pH 6.5) containing 1.25 mM GSH (0.8 ml) and 10 mM 1-chloro-2,4-dinitrobenzene in 40% ethanol (0.1 ml). The reaction mixture was incubated at 25 °C for 10 min and monitored at 340 nm.

2.6. SOD2 activity

SOD2 activity was measured using a Superoxide Dismutase Assay kit (Cayman Chemical, Ann Arbor, MI). The method utilizes tetrazolium salt to quantify the superoxide radicals generated by xanthine oxidase and hypoxanthine. The standard curve was generated using a quality controlled SOD standard in the kit. SOD2 activity was determined in the presence of potassium cyanide to inhibit SOD1 activity.

2.7. Protein carbonyl content

Plasma protein carbonyl content was measured using an OxiSelect Protein Carbonyl ELISA kit (Cell Biolabs, Tokyo, Japan) as described previously (Yoshikawa et al., 2009).

2.8. Real-time reverse transcription (RT)-PCR

Total hepatic RNA was isolated using RNAiso according to the manufacturer's instructions. Human CYP2C8, CYP3A4, SULT1A1, UGT1A1 and GAPDH mRNA levels were quantified by real-time RT-PCR. Total RNA (4 μg) and 150 ng random hexamer were mixed and incubated at 70 °C for 10 min. An RNA solution was added to a reaction mixture that contained 100 units of ReverTra Ace, reaction buffer and 0.5 mM dNTPs in a final volume of 40 μl. The reaction mixture was incubated at 30 °C for 10 min, 42 °C for 1 h, and then heated at 98 °C for 10 min to inactivate the enzyme. Real-time RT-PCR was performed using the Mx3000P (Stratagene, La Jolla, CA). The PCR mixture contained 1 μl of template cDNA, SYBR Premix Ex Taq solution, and 10 pmol of sense and antisense primers. The human-specific primer sequences used in this study are shown in Table 2. The amplified products were monitored directly by measuring the intensity of the SYBR Green I dye (Molecular Probes, Eugene, OR) that binds to the PCR amplified double-stranded DNA.

2.9. Immunoblot analysis

SDS-polyacrylamide gel electrophoresis and immunoblot analysis of human CYP2C8 and CYP3A were performed according to Katoh et al. (2004). The liver microsomes (2 or 20 μg) were separated on 10% polyacrylamide gel and transferred electrophoretically to a polyvinylidene difluoride membrane. Recombinant human P450s were applied as standards. Biotinylated anti-rabbit or goat IgG and a Vectastain ABC kit (Vector Laboratories, Burlingame, CA) were used for diaminobenzidine staining. It was confirmed that the human P450 antibodies in this experimental condition did not cross-react with the mouse orthologs.

Table 1
Chimeric mice used in this study.

Group	Mouse no.	Age at 1st dose (week)	hAlb concentration in the blood (mg/ml)	Approximate RI (%)
Control	1	13	9.6	80
	2	13	11.6	85
	3	13	9.1	78
	4	11	8.0	75
	5	12	9.3	79
	6	12	11.6	85
Tro 1000 mg/kg (14 days)	7	13	11.7	85
	8	13	9.6	80
	9	13	9.1	78
	10	14	9.7	80
	11	13	9.6	80
Tro 250 mg/kg (28 days)	S1	12	9.3	79
	S2	12	8.4	76
	S3	12	10.5	82
	S4	12	9.0	78
	S5	12	10.6	83
Tro 500 mg/kg (28 days)	S6	12	9.7	80
	S7	12	9.6	80
	S8	11	9.1	78
	S9	12	8.2	75
	S10	15	9.5	80
Tro 1000 mg/kg (23 days)	12	15	14.9	92
	13	14	12.3	87
	14	14	14.6	92
	15	15	8.3	76
BSO (14 days)	16	13	10.3	82
	17	13	9.2	79
	18	13	11.6	85
BSO + Tro 1000 mg/kg (14 days)	19	13	8.7	77
	20	13	10.3	82
	21	13	9.2	79

RI, replacement index.

Table 2
Sequence of primers for real-time RT-PCR analyses.

Primer	Sequence
CYP2C8 S[a]	5′-AGATCAGAATTTCTCACCC-3′
CYP2C8 AS[a]	5′-AACTTCGTGTAAGAGCAACA-3′
CYP3A4 S[a]	5′-CCAAGCTATGCTCTTCACCG-3′
CYP3A4 AS[a]	5′-TCAGGTCCACTTACGGTGC-3′
SULT1A1 S	5′-ATGGAGACTCTGAAAGACACACCGG-3′
SULT1A1 AS	5′-TGTGCTGAACCACGAAGTCCACG-3′
UGT1A1 S[b]	5′-CCTTGCCTCAGAATTCCTTC-3′
UGT1A1 AS[b]	5′-ATTGATCCCAAAGAGAAAACCAC-3′
GAPDH S[a]	5′-CCAGGGCTTTTAACTC-3′
GAPDH AS[a]	5′-GCTCCCCCCTGCAAATGA-3′

S, sense primer; AS, antisense primer.
[a] From Katoh et al. (2004).
[b] From Izukawa et al. (2009).

2.10. CYP2C8 and CYP3A4 activities

Liver microsomes from the chimeric or control mice were prepared as described previously (Katoh et al., 2004) and stored at −80 °C until analysis. The protein concentration was determined using Bradford assay reagent (Bio-Rad, Hercules, CA) with bovine γ globulin as the standard. The typical incubation mixtures (total volume, 0.2 ml) consisted of microsomes in 100 mM potassium phosphate buffer (pH 7.4) containing an NADPH-generating system (0.5 mM $NADP^+$, 5 mM glucose 6-phosphate, 5 mM $MgCl_2$, and 1 unit/ml glucose-6-phosphate dehydrogenase) and a substrate.

Paclitaxel 6α-hydroxylase activity was determined by the method of Willey et al. (1993), with slight modifications. The concentrations of the microsomes and paclitaxel were 0.5 mg/ml and 20 μM, respectively. The reaction mixture was incubated at 37 °C for 10 min, and terminated by adding 1.0 ml of dichloromethane. Testosterone (10 μl of 100 μM) was added as an internal standard. After centrifugation at 900 × *g* for 10 min, the organic phase (500 μl) was evaporated under a gentle stream of nitrogen at 40 °C. The residue was redissolved in 200 μl of mobile phase and then 100-μl portion of the sample was subjected to high-performance liquid chromatography (HPLC). The product formation was determined with a Mightysil RP-8 C8 GP column (5-μm particle size, 4.6 i.d. × 150 mm; Kanto Chemical, Tokyo, Japan). The mobile phase (45% acetonitrile/20 mM ammonium acetate) was used under isocratic condition. The flow rate was 1.0 ml/min, and the column temperature was 35 °C. The eluent was monitored at 227 nm. The quantification of 6α-hydroxypaclitaxel was performed by comparing the HPLC peak heights to that of authentic standards with reference to an internal standard. The retention time of 6α-hydroxypaclitaxel and paclitaxel was 9.0 and 14.7 min, respectively.

The dexamethasone 6-hydroxylase activity was determined according to the method of Tomlinson et al. (1997), with slight modifications. The concentrations of microsomes and dexamethasone were 1.0 mg/ml and 100 μM, respectively. The reaction mixture (total volume, 0.2 ml) was incubated at 37 °C for 30 min, and terminated by adding 1.5 ml of ice-cold ethyl acetate. 6-Hydroxytestosterone (10 μl of 10 ng/μl) was added as an internal standard. After centrifugation at 900 × *g* for 10 min, the organic phase (500 μl) was evaporated under a gentle stream of nitrogen at 40 °C. The residue was redissolved in 200 μl of mobile phase and then 100-μl portion of the sample was subjected to HPLC. The product formation was determined with a Mightysil RP-8 C8 GP column (5-μm particle size, 4.6 i.d. × 150 mm; Kanto Chemical). The mobile phase (23% acetonitrile/0.015% formic acid) was used under isocratic condition. The flow rate was 1.0 ml/min, and the column temperature was 35 °C. The eluent was monitored at 243 nm. The dexamethasone 6-hydroxylase activity was quantified using a standard curve of dexamethasone because we could not obtain pure 6-hydroxydexamethasone. The retention time of 6-hydroxydexamethasone was confirmed using the incubation product of recombinant CYP3A4 and dexamethasone. The retention time of 6-hydroxydexamethasone and dexamethasone was 4.8 and 37.7 min respectively. The final concentration of the solvent in the incubation mixture was less than 1%.

2.11. Statistical analysis

Statistical analyses between multiple groups were performed using one-way analysis of variance (ANOVA), followed by Dunnett's *post hoc* test. Comparisons between two groups were performed using two-tailed Student's *t*-test. A value of $P < 0.05$ was considered statistically significant.

Table 3
Serum biochemical parameters in toroglitazone and/or BSO-administered chimeric mice.

Group	Mouse no.	ALT (U/l)			AST (U/l)		LDH (U/l)		T-Bil (mg/dl)		D-Bil (mg/dl)	
		Initial	Final		Final		Final		Final		Final	
Control	1	108	77		147		1366		0.8		0.1	
	2	90	56		83		2884		0.7		0.1	
	3	140	139		212		1386		0.8		0.1	
	4	87	137		152		1554		0.8		ND	
	5	88	79		126		832		0.9		ND	
	6	92	106		188		1122		0.8		ND	
	Mean ± SD	101 ± 21	99 ± 34	[1.0]	151 ± 46	[1.0]	1524 ± 712	[1.0]	0.8 ± 0.1	[1.0]	0.1 ± 0.0	[1.0]
Tro 1000 mg/kg (14 days)	7	64	67		170		3600		0.9		0.1	
	8	96	233	R	345		2520		1.5		0.4	
	9	144	218	R	283		861		1.0		0.1	
	10	79	167	R	188		1724		0.8		0.1	
	11	39	64		145		897		0.9		0.1	
	Mean ± SD	84 ± 39	150 ± 81	[1.5]	226 ± 84	[1.5]	1920 ± 1161	[1.3]	1.0 ± 0.3	[1.3]	0.2 ± 0.1	[2.0]
	R (n=3)	106 ± 34	206 ± 35**	[2.1]	272 ± 79	[1.8]	1702 ± 830	[1.1]	1.1 ± 0.4	[1.4]	0.2 ± 0.2	[2.0]
Tro 250 mg/kg (28 days)	S1	62	344	R	361		2256		0.9		ND	
	S2	71	182		250		902		0.9		ND	
	S3	75	70		165		1498		0.7		ND	
	S4	59	146	R	186		823		0.8		ND	
	S5	80	111		130		667		0.8		ND	
	Mean ± SD	69 ± 9	171 ± 105	[1.7]	218 ± 91	[1.4]	1229 ± 655	[0.8]	0.8 ± ±0.1	[1.0]	0.1 ± 0.0	[1.0]
Tro 500 mg/kg (28 days)	S6	66	108		144		779		0.7		ND	
	S7	78	205	R	318		1126		0.7		ND	
	S8	79	48		93		531		0.6		ND	
	S9	81	91		114		487		0.7		ND	
	S10	71	171	R	170		982		0.6		ND	
	Mean ± SD	75 ± 6	125 ± 63	[1.3]	168 ± 89	[1.1]	781 ± 278	[0.5]	0.7 ± 0.1	[0.9]	0.1 ± 0.0	[1.0]
Tro 1000 mg/kg (23 days)	12	79	504	R	452		1566		0.6		0.1	
	13	70	221	R	260		1550		0.7		0.1	
	14	84	345	R	410		1274		0.7		0.1	
	15	113	97		138		729		0.7		ND	
	Mean ± SD	87 ± 19	292 ± 174	[2.9]	315 ± 144	[2.1]	1280 ± 391	[0.8]	0.7 ± 0.1	[0.9]	0.1 ± 0.0	[1.0]
	R (n=3)	78 ± 7	357 ± 142**	[3.6]	374 ± 101**	[2.5]	1463 ± 164	[1.0]	0.7 ± 0.1	[0.9]	0.1 ± 0.0	[1.0]
BSO (14 days)	16	58	51		102		1728		0.8		0.2	
	17	65	91		131		1206		0.6		0.1	
	18	53	38		123		1504		0.7		0.1	
	Mean ± SD	59 ± 6	60 ± 28	[0.6]	119 ± 15	[0.8]	1479 ± 262	[1.0]	0.7 ± 0.1	[0.9]	0.1 ± 0.1	[1.0]
BSO + Tro 1000 mg/kg (14 days)	19	117	59		175		1572		0.7		0.2	
	20	55	55		105		891		0.6		ND	
	21	76	39		144		836		0.8		0.1	
	Mean ± SD	83 ± 32	51 ± 11	[0.5]	141 ± 35	[0.9]	1100 ± 410	[0.7]	0.7 ± 0.1	[0.9]	0.2 ± 0.1	[2.0]

Each parameter except initial value was measured 24 h after the last troglitazone administration.
Differences compared to the control group were considered significant at $^{**}P < 0.01$.
ND, not detected; R, responder; score in parenthesis, ratio to the control.

3. Results

3.1. TRO caused liver injury in chimeric mice with a humanized liver

TRO was orally administered to female chimeric mice at a dose of 250 mg/kg/day for 28 days (Tro 250-28 day), 500 mg/kg/day for 28 days (Tro 500-28 day), and 1000 mg/kg/day for 14 days (Tro 1000-14 day) or 23 days (Tro 1000-23 day) in a non-fasting condition. BSO (10 mM in drinking water) was treated alone or with Tro administration for 14 days. The initial serum ALT levels ranged from 39 to 144 U/l among all animals (Table 3). The final ALT levels in the Tro 250-28 day (171 ± 105 U/l), Tro 500-28 day (125 ± 63 U/l), Tro 1000-14 day (150 ± 81 U/l) and Tro 1000-23 day (292 ± 174 U/l) groups increased by 1.7-, 1.3-, 1.5- and 2.9-fold, respectively compared to the control group (99 ± 34 U/l). Two out of five mice in both Tro 250-28 day and Tro 500-28 day groups, three out of five mice in the Tro 1000-14 day group and three out of four mice in the Tro 1000-23 day group showed increased ALT levels of more than 144 U/l, the highest initial ALT level among all mice. These mice were termed responders (R) in Table 3. The average values of ALT levels in Tro 250-28 day and Tro 500-28 day groups are a little higher than the control group, however there is no clear dose–response in these values. These results suggest that the dose level of 1000 mg/kg is required for the onset of troglitazone-induced liver injury in the chimeric mice. Therefore, we put focus on the results from 1000 mg/kg dose groups in the subsequent analyses. The final ALT levels in responders in the Tro 1000-14 day and Tro 1000-23 day groups were significantly higher than those in the control group by 2.1- and 3.6-fold, respectively (Fig. 1). For the subsequent analyses, the data from the responders (R) in Tro 1000-14 day and Tro 1000-23 day groups were compared to those in the control group.

The final AST level in the Tro 1000-23 day group was significantly higher than that in the control group by 2.5-fold. The final serum LDH, T-Bil and D-Bil levels in the Tro 1000-14 day and Tro 1000-23 day groups were unchanged compared to the control group (Table 3). The LDH, T-Bil and D-Bil levels in the Tro 1000-23 day group were lower than those in the Tro 1000-14 day group. Both in the BSO alone and BSO- and Tro-administered groups, serum ALT, AST, LDH, T-Bil and D-Bil levels were unchanged compared to the levels in the control group (Table 3 and Fig. 1).

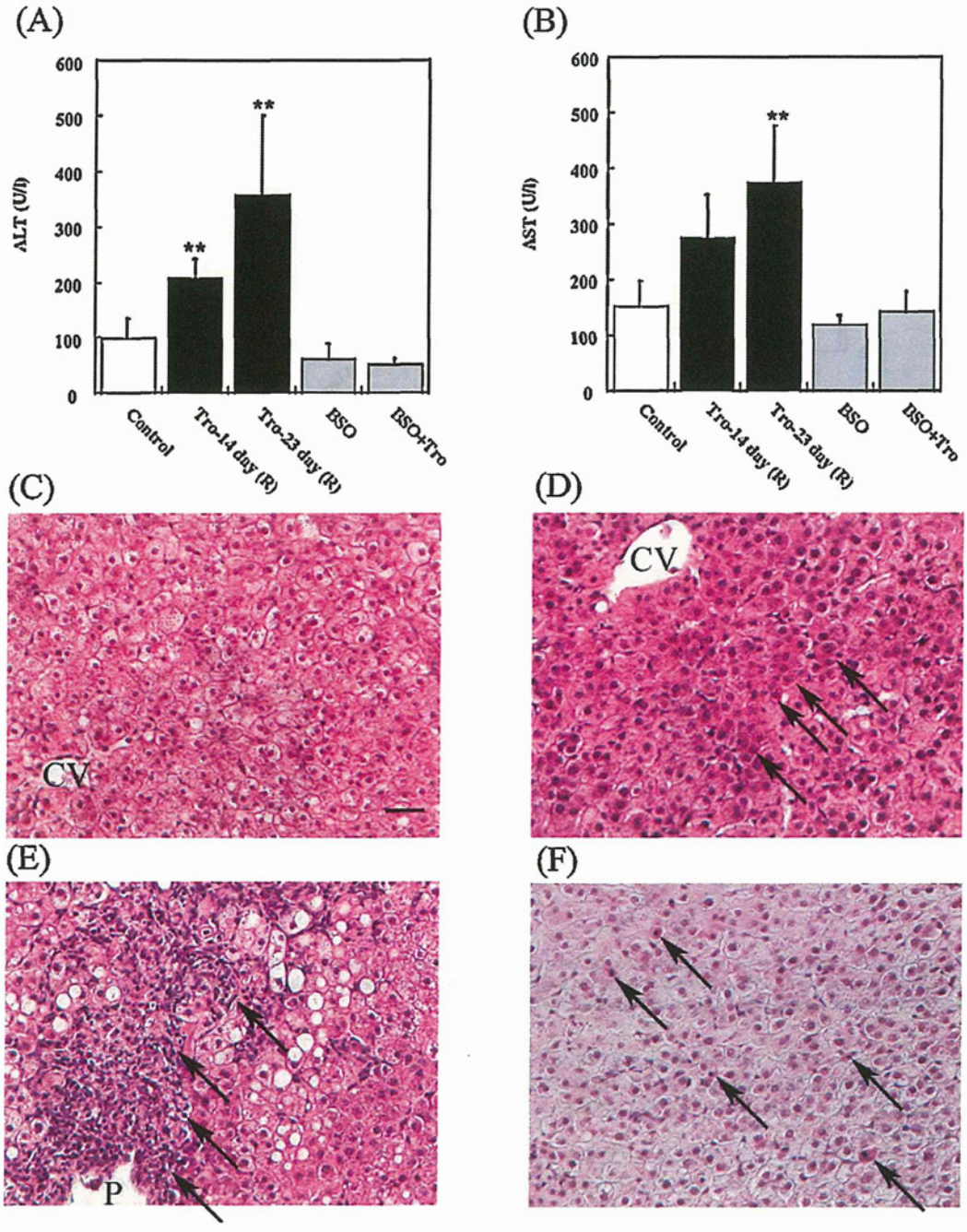

Fig. 1. Changes in the serum ALT and AST levels and liver histology by Tro and/or BSO administration in chimeric mice. The chimeric mice were orally administered Tro (1000 mg/kg/10 ml, suspended in 0.5% CMC) once daily for 14 or 23 days in a non-fasting condition, and 0.5% CMC was administered once daily for 14 days as a control. BSO (10 mM in drinking water) was also given alone or with Tro administration for 14 days. (A) ALT and (B) AST were measured 24 h after the last administration. The data are shown as the mean ± SD of the results from 3 to 6 mice. In the Tro-14 day ($n = 3$) and Tro-23 day ($n = 3$) group, the data are from the responder chimeric mice (R). The differences compared to the control group ($n = 6$) were considered significant at $^{**}P < 0.01$. (C–F) The liver specimens from the chimeric mice were sampled 24 h after the last Tro administration and subsequently stained with H&E. The human hepatocytes in the control chimeric mouse had a clear cytoplasm and no cellular infiltration (C, mouse no. 2). The arrows indicate an eosinophilic change of human hepatocytes (D, mouse no. 12, Responder), neutrophil infiltration (E, mouse no. 13, Responder) and necrosis of human hepatocytes (F, mouse no. 14, Responder). CV: central vein; P: portal vein; Bars: 40 μm (C–F are the same scale).

In the control chimeric mouse, a clear cytoplasm and no cellular infiltration were observed in the human hepatocytes in the liver tissue of the chimeric mice (Fig. 1C). In the responder chimeric mice, the human hepatocytes in the liver tissue showed slight eosinophilic changes (Fig. 1D), neutrophil infiltration surrounding the area of the portal vein (Fig. 1E) and scattered single cell necrosis (Fig. 1F) after Tro administration.

3.2. Oxidative stress responses in chimeric mice with a humanized liver

In both the Tro 1000-14 day and Tro 1000-23 day groups, the hepatic GSH contents were significantly higher in the Tro-administered responder mice by approximately 2-fold than in the control group (Fig. 2A). GST activities, SOD2 activities and the

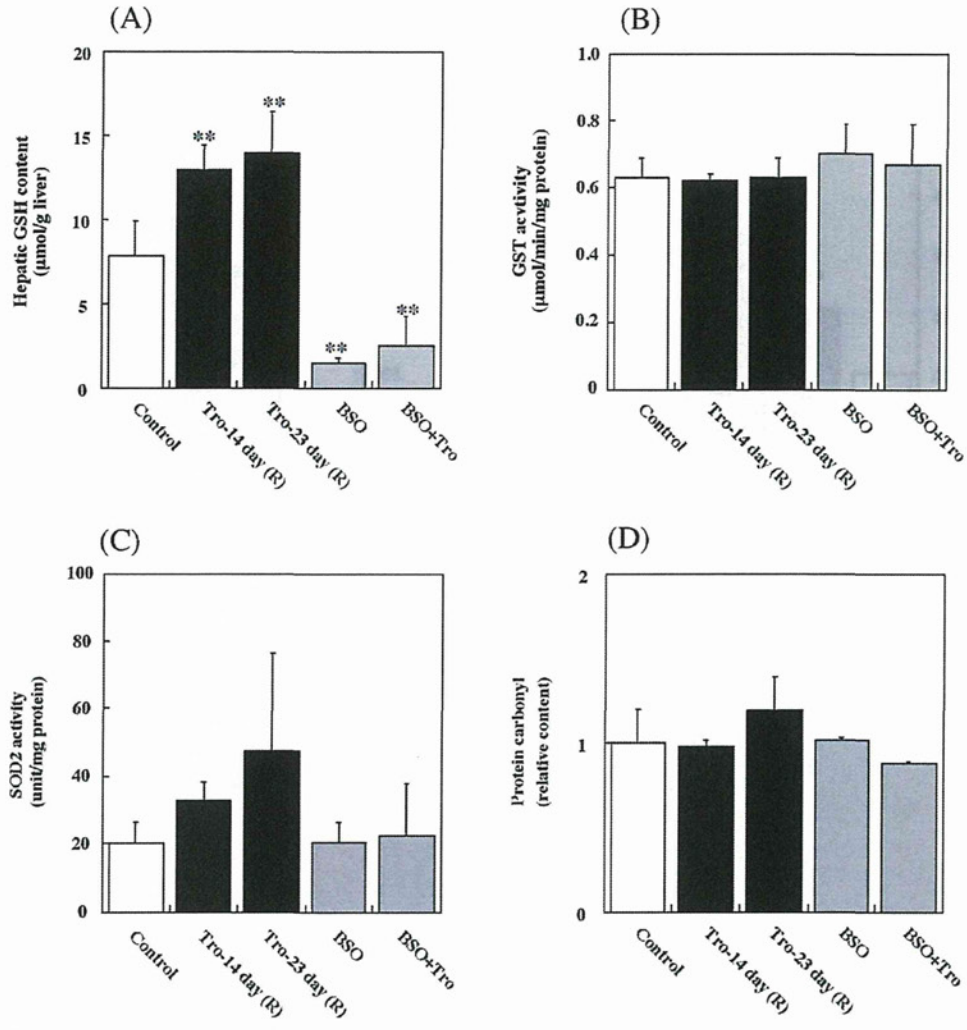

Fig. 2. Changes in the hepatic GSH content (A), GST activity (B), SOD2 activity (C), and plasma protein carbonyl content (D) in the chimeric mice that were administered Tro and/or BSO. The data are shown as the mean ± SD of the results from 3 to 6 mice. In the Tro-14 day and Tro-23 day groups, the data are from the responder chimeric mice. The differences compared to the control group were considered significant at $^{**}P < 0.01$.

protein carbonyl content showed no significant change following Tro administration (Fig. 2B–D). SOD2 activity in the Tro 1000-23 day group was higher than in the control: however, the difference in activity was not significant.

The effects of the GSH-lowering agent BSO on oxidative stress in the chimeric mice were evaluated. The hepatic GSH contents were significantly decreased in the BSO group by approximately 0.2-fold compared to the control group. However, in the BSO and Tro-administered group, the GSH content was suppressed by Tro administration. The hepatic GST activities were unchanged with the administration of BSO alone or BSO and Tro administration. The administration of BSO and Tro showed no change in SOD2 activity. The protein carbonyl contents also showed no change among the groups in this study (Fig. 2D). These results suggested that Tro induced the GSH synthesis enzyme, which was inhibited by BSO.

3.3. *Effect of Tro and/or BSO administration on the expression of drug metabolizing enzymes in the chimeric mice with a humanized liver*

We determined the expression levels of drug metabolizing enzymes, which are involved in the metabolism of Tro in human. The expression level of human CYP2C8 mRNA (Fig. 3A) was increased with the administration of Tro and/or BSO. The expression level of CYP2C8 protein (Fig. 3B) and paclitaxel 6a-hydroxylase activities (Fig. 3C) were significantly increased by the administration of Tro. The expression levels of CYP3A4 mRNA (Fig. 4A) and protein (Fig. 4B) also tended to increase with the administration of Tro and/or BSO. Dexamethasone 6-hydroxylase activities were significantly increased by the administration of Tro and/or BSO. Therefore, these results clearly demonstrated that Tro induced CYP2C8 and CYP3A4 in the liver of the chimeric mice with a humanized liver. Interestingly, the administration of BSO alone also induced both enzymes. Based on these data, enzyme induction is unlikely to be involved in Tro-induced liver injury. In addition, we found that Tro induced the expression level of human UGT1A1 (Fig. 5B) mRNA. The administration of BSO and/or Tro also induced the expression level of UGT1A1 mRNA.

4. Discussion

During the preclinical development and following the withdrawal of Tro, pharmaceutical companies performed numerous toxicity studies using mice, rats and monkeys (Watanabe et al.,

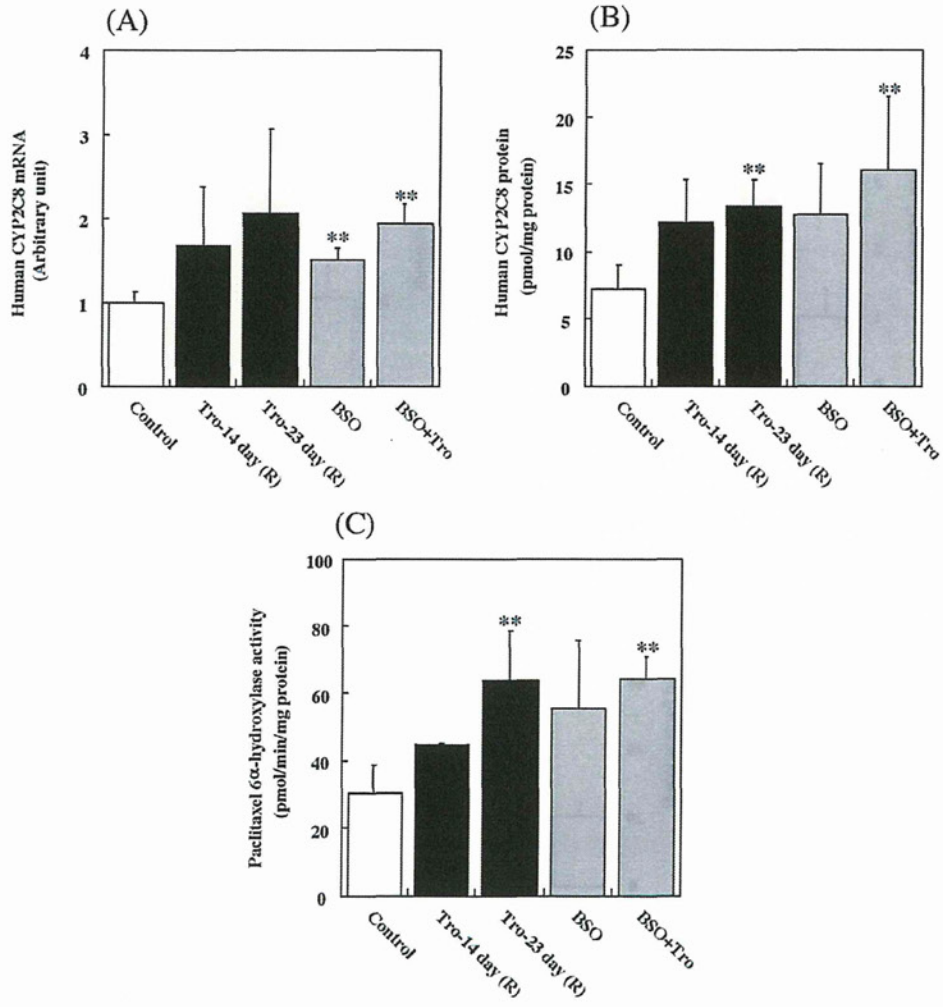

Fig. 3. Changes in the expression level of human CYP2C8 mRNA (A), protein content (B), and enzyme activity (C) in the liver of chimeric mice that were administered Tro and/or BSO. Paclitaxel 6a-hydroxylase activity was catalyzed by CYP2C8 and measured using 20 μM paclitaxel as a substrate. The data are shown as the mean ± SD of the results from 3 to 6 mice. In the Tro-14 day and Tro-23 day groups, the data are from the responder chimeric mice. The differences compared to the control group were considered significant at $^{**}P < 0.01$.

1999). In these toxicity studies, Tro was administered at a dose of 800 mg/kg/day for 24 months to mice, 1200 mg/kg/day for 12 months to rats and 1200 mg/kg/day for 12 months to monkeys, but no signs of liver dysfunction were confirmed (Watanabe et al., 1999). Chimeric mice with a humanized liver are suitable for *in vivo* studies utilizing human hepatocytes. The present study used chimeric mice with a humanized liver and successfully demonstrated Tro-induced liver with the once daily oral administration for 14 and 23 days of 1000 mg/kg Tro. The development of Tro-induced liver injuries in the responder chimeric mice was confirmed by the significant increase in the final serum ALT and AST levels that occurred in an administration-duration-dependent manner (Fig. 1A and B), the eosinophilic changes (Fig. 1D) and cellular infiltrations in the liver tissue (Fig. 1E) and single cell necrosis of human hepatocytes (Fig. 1F). Using the same chimeric mice, Schulz-Utermoehl et al. (2012) did not demonstrate liver injury administering a once daily oral dose for 7 days of 300 and 600 mg/kg Tro, and no significant differences in the pharmacokinetics parameters of C_{max} or AUC were observed following doses of Tro at 300 and 600 mg/kg. These evidences support our results that 250 and 500 mg/kg of Tro was insufficient for the onset of Tro-induced liver injury in the chimeric mice when dosed once daily for 28 days. Both the dose level and the dosing period will be essential factors for the onset of Tro-induced liver injury.

The increase of serum transaminases was considered to be derived from the human hepatocytes, which was supported by the histological changes. However, we were unable to distinguish human ALT from mouse ALT quantitatively (data not shown). Conversely, two out of five mice in the Tro 1000-14 day group and one out of four mice in the Tro 1000-23 day group did not show hepatic injury. As shown in Table 1, the chimeric mice exhibited a hAlb concentration of 8.0–14.9 mg/ml and 75–92% of RI and received transplanted human hepatocytes from the same donor. The hAlb levels of the non-responder chimeric mice ranged from 8.2 (RI: 75%) to 11.7 mg/ml (RI; 85%), and appeared to not be critically different from the hAlb levels of the responder chimeric mice, which ranged from 9.0 (RI: 78%) to 14.9 (RI: 92%). Therefore, it was considered that the individual difference in the onset of liver injury among the mice would depend on other factors as discussed below.

It has been reported that the double null mutant of GSTT1 and GSTM1 in humans correlated with Tro-associated abnormal increases in ALT levels (odds ratio, 3.692; 95% confidence interval, 1.354–10.066; $P = 0.008$) (I. Watanabe et al., 2003). However, the present study revealed that the difference in the onset of liver injury

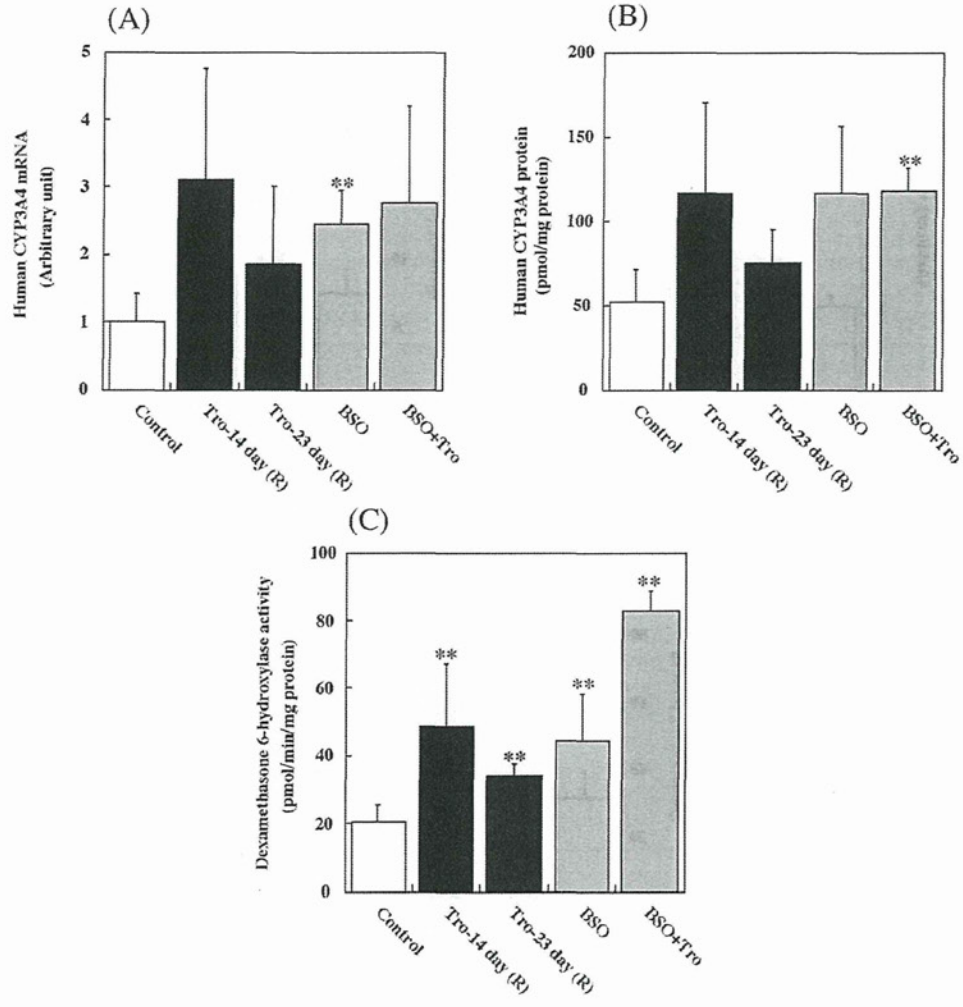

Fig. 4. Changes in the expression level of human CYP3A4 mRNA (A), protein content (B), and enzyme activity (C) in the liver of chimeric mice administered Tro and/or BSO. Dexamethasone 6-hydroxylase activity was catalyzed by CYP3A4 and measured using 100 μM dexamethasone as a substrate. The data are shown as the mean ± SD of the results from 3 to 6 mice. In the Tro-14 day and Tro-23 day groups, the data are from the responder chimeric mice. The differences compared to the control group were considered significant at $^{**}P < 0.01$.

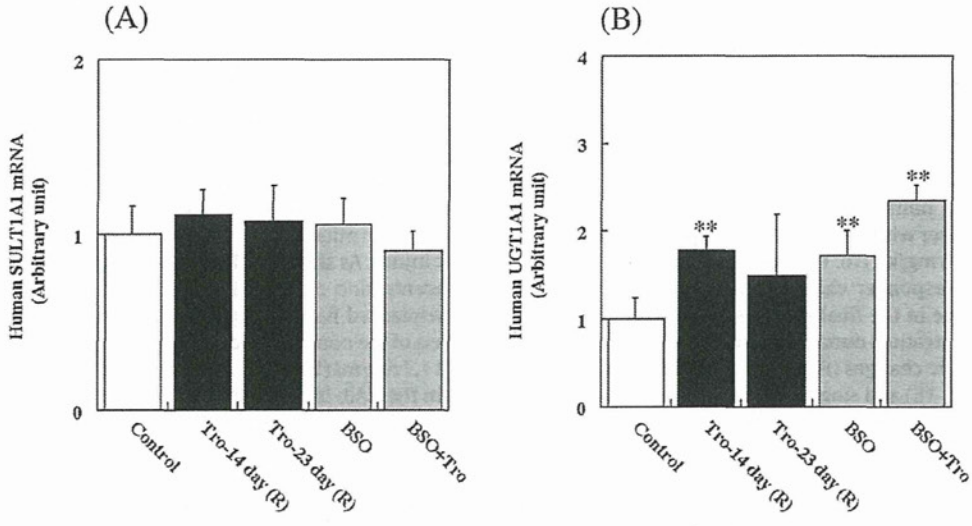

Fig. 5. Changes in the expression level of human SULT1A1 mRNA (A) and human UGT1A1 mRNA expression (B) in the liver of chimeric mice that were administered Tro and/or BSO. The data are shown as the mean ± SD of the results from 3 to 6 mice. In the Tro-14 day and Tro-23 day groups, the data are from the responder chimeric mice. The differences compared to the control group were considered significant at $^{**}P < 0.01$.

could be Tro-induced in the chimeric mice with genetically identical human hepatocytes genotyped to wild-type GSTT1 and GSTM1 (data not shown). It is conceivable that the double null mutant of GSTT1 and GSTM1 is unlikely to be a risk factor, which was recently suggested by Usui et al. (2011) using cytotoxicity assays of human hepatocytes.

BSO was administered to evaluate the effects of GSH depletion on Tro-induced liver injury. The suspected active metabolite of Tro, a quinone metabolite, has been reported to not react directly with GSH, and it can be further metabolized to an *O*-quinone methide or undergo ring opening to produce additional highly electrophilic intermediates (Kassahun et al., 2001). However, in this study, neither the serum biochemical analyses nor the histological examinations showed evidence of liver injury in the BSO alone and BSO- and Tro-administered group, whereas the hepatic GSH contents decreased approximately 0.2- and 0.4-fold in these groups, respectively compared to the control group (Fig. 2A). Furthermore, hepatic GST activities were maintained in all groups (Fig. 2B). Although the results in this study appear to not support the general understanding of scavenging systems for reactive metabolites, it was suggested that the onset of Tro-induced liver injury was independent of scavenging systems associated with hepatic GSH. Interestingly, the hepatic GSH contents significantly increased with the administration of Tro (Fig. 2A), although the functional mechanism in relation to the onset of liver injury was unclear.

SOD2 activity and protein carbonyl contents were measured to clarify whether an increase in oxidative stress might be associated with the onset of Tro-induced liver injury (Fig. 2C and D), as reported in a study using *SOD2*$^{+/-}$ mice (Ong et al., 2007). In the *SOD2*$^{+/-}$ mouse study, the increase in the serum AST level and the degeneration of hepatocytes were observed when 30 mg/kg of Tro was intraperitoneally administered once per day for 4 weeks (Ong et al., 2007). However, the phenomenon was not reproduced by other group (Fujimoto et al., 2009) despite the administered to the same dose to the same *SOD2*$^{+/-}$ mice. We found that SOD2 activities were tended to increase in the Tro-23 day group. Furthermore, the protein carbonyl contents were unchanged. These results suggest that oxidative stress may not involved in Tro-induced liver injury in the chimeric mice.

In humans, Tro is metabolized by three pathways, *i.e.*, sulfation by SULT1A1 (Honma et al., 2002), glucuronidation by UGT1A1 (Yoshigae et al., 2000), and oxidation to form a quinone metabolite (M3) by CYP2C8 and CYP3A4 (Yamazaki et al., 1999; Yamamoto et al., 2002). Recently, the chimeric mice were confirmed to show the unique profiles in metabolism of Tro when compared to SCID mice (Schulz-Utermoehl et al., 2012). A total of 32 putative metabolites plus Tro were detected in blood from the chimeric mice, with 14 (M1, M4–M10, M12 and M17–M21) of these metabolites detected only in blood from the chimeric mice. Of these 14 metabolites, 4 (M4, M7, M8 and M12) were also detected only in liver extracts from the chimeric mice. The relative concentrations of the glucuronide metabolite (M13) were higher in liver preparations from SCID mice. These findings suggested the chimeric mice possess metabolically active human hepatocytes and have a potential to generate unique human metabolite (Schulz-Utermoehl et al., 2012). The involvement of a sulfo-conjugate in Tro-induced liver injury was suggested in *in vitro* study by Saha et al. (2010) who reported that a sulfo-conjugate of Tro exerted direct toxic effects on human hepatocytes, possibly *via* oxidative stress induction. In contract, the expression level of SULT1A1 mRNA was not changed in this study, suggesting the difference effect of Tro between *in vivo* and *in vitro* study.

We found that CYP2C8 and CYP3A4 were induced by the administration of Tro, as previously reported (Sahi et al., 2003). However, the onset of the Tro-induced liver injury was considered independent of the induction of these drug-metabolizing enzymes because enzyme induction was also observed in the BSO alone- and BSO and Tro-administered group. The cause of the moderate induction of CYP3A4 in the Tro-23 day group compared with the Tro-14 day group remains unclear. However, it was reported that hepatic expression levels of proinflammatory cytokines, tumor necrosis factor (TNF) α and interleukin (IL)-6 and chemokines were increased in the mouse model of drug-induced liver injury (Toyoda et al., 2011, 2012). TNFα was also identified to be involved in the down-regulation of CYP3A11 and CYP3A25 in mouse liver (Kinloch et al., 2011). In addition, IL-6 was reported to down-regulate the expression of CYP3A4 *via* pregnane X receptor in human hepatocytes (Yang et al., 2010). Taking these recent reports into consideration, chronic hepatic inflammation in the Tro-23 day group might be a causal factor for the decreased expression level of CYP3A4 in this study.

As shown in Fig. 5B, UGT1A1 appears unrelated to the onset of the Tro-induced liver injury because significant increases in human UGT1A1 mRNA expression were observed not only in the Tro-14 day group but also in the BSO alone and BSO- and Tro-administered groups.

Notably, the chimeric mice were generated using an uPA$^{+/+}$/SCID mouse line, which is defective in functional T and B lymphocytes (Bosma et al., 1983). Tro-induced liver injury in the chimeric mice could be successfully produced when free from T and B lymphocyte-mediated immune responses. However, SCID mice were once daily orally administered Tro at 300 and 600 mg/kg doses for 7 days and showed no change in ALT and AST levels (Schulz-Utermoehl et al., 2012). Further investigations comparing SCID mice and the chimeric mice with a humanized liver are necessary.

Idiosyncratic liver injury is a critical issue for clinical practice and drug development. Thus, numerous attempts have been made to establish a method for predicting idiosyncratic liver injury in human. The present study succeeded in demonstrating Tro-induced liver injury using chimeric mice with a humanized liver. The advantage of this mouse model is to enable human hepatocytes to be examined in an *in vivo* environment. The chimeric mice with a humanized liver will be a useful tool to investigate the unsolved mechanism of idiosyncratic Tro-induced hepatic injury.

Funding information

Health and Labor Sciences Research Grants from the Ministry of Health, Labor, and Welfare of Japan (H23-BIO-G001).

Conflict of interest statement

The authors declare that there are no conflicts of interest.

References

Bedoucha, M., Atzpodien, E., Boelsterli, U.A., 2001. Diabetic KKAy mice exhibit increased hepatic PPARγ1 gene expression and develop hepatic steatosis upon chronic treatment with antidiabetic thiazolidinediones. Journal of Hepatology 35, 17–23.

Bosma, G.C., Custer, R.P., Bosma, M.J., 1983. A severe combined immunodeficiency mutation in the mouse. Nature 301, 527–530.

Fujimoto, K., Kumagai, K., Ito, K., Arakawa, S., Ando, Y., Oda, S., Yamoto, T., Manabe, S., 2009. Sensitivity of liver injury in heterozygous Sod2 knockout mice treated with troglitazone or acetaminophen. Toxicologic Pathology 37, 193–200.

Habig, W.H., Pabst, M.J., Jakoby, W.B., 1974. Glutathione S-transferases. The first enzymatic step in mercapturic acid formation. Journal of Biological Chemistry 249, 7130–7139.

He, K., Talaat, R.E., Pool, W.F., Reily, M.D., Reed, J.E., Bridges, A.J., Woolf, T.F., 2004. Metabolic activation of troglitazone: identification of a reactive metabolite and mechanisms involved. Drug Metabolism and Disposition: The Biological Fate of Chemicals 32, 639–646.

Honma, W., Shimada, M., Sasano, H., Ozawa, S., Miyata, M., Nagata, K., Ikeda, T., Yamazoe, Y., 2002. Phenol sulfotransferase, ST1A3, as the main enzyme catalyzing sulfation of troglitazone in human liver. Drug Metabolism and Disposition: The Biological Fate of Chemicals 30, 944–949.

Izukawa, T., Nakajima, M., Fujiwara, R., Yamanaka, H., Fukami, T., Takamiya, M., Aoki, Y., Ikushiro, S., Sakaki, T., Yokoi, T., 2009. Quantitative analysis of UDP-glucuronosyltransferase (UGT) 1A and UGT2B expression levels in human livers. Drug Metabolism and Disposition: The Biological Fate of Chemicals 37, 1759–1768.

Jia, D.M., Tabaru, A., Akiyama, T., Abe, S., Otsuki, M., 2000. Troglitazone prevents fatty changes of the liver in obese diabetic rats. Journal of Gastroenterology and Hepatology 15, 1183–1191.

Kassahun, K., Pearson, P.G., Tang, W., McIntosh, I., Leung, K., Elmore, C., Dean, D., Wang, R., Doss, G., Baillie, T.A., 2001. Studies on the metabolism of troglitazone to reactive intermediates in vitro and in vivo. Evidence for novel biotransformation pathways involving quinone methide formation and thiazolidinedione ring scission. Chemical Research in Toxicology 14, 62–70.

Katoh, M., Matsui, T., Nakajima, M., Tateno, C., Kataoka, M., Soeno, Y., Horie, T., Iwasaki, K., Yoshizato, K., Yokoi, T., 2004. Expression of human cytochromes P450 in chimeric mice with humanized liver. Drug Metabolism and Disposition: The Biological Fate of Chemicals 32, 1402–1410.

Katoh, M., Matsui, T., Okumura, H., Nakajima, M., Nishimura, M., Naito, S., Tateno, C., Yoshizato, K., Yokoi, T., 2005. Expression of human phase II enzymes in chimeric mice with humanized liver. Drug Metabolism and Disposition: The Biological Fate of Chemicals 33, 1333–1340.

Katoh, M., Sawada, T., Soeno, Y., Nakajima, M., Tateno, C., Yoshizato, K., Yokoi, T., 2007. In vivo drug metabolism model for human cytochrome P450 enzyme using chimeric mice with humanized liver. Journal of Pharmaceutical Sciences 96, 428–437.

Kinloch, R.D., Lee, C.M., van Rooijen, N., Morgan, E.T., 2011. Selective role for tumor necrosis factor-α, but not interleukin-1 or Kupffer cells, in down-regulation of CYP3A11 and CYP3A25 in livers of mice infected with a noninvasive intestinal pathogen. Biochemical Pharmacology 82, 312–321.

Nishimura, M., Yoshitsugu, H., Yokoi, T., Tateno, C., Kataoka, M., Horie, T., Yoshizato, K., Naito, S., 2005. Evaluation of mRNA expression of human drug-metabolizing enzymes and transporters in chimeric mouse with humanized liver. Xenobiotica 35, 877–890.

Ong, M.M., Latchoumycandane, C., Boelsterli, U.A., 2007. Troglitazone-induced hepatic necrosis in an animal model of silent genetic mitochondrial abnormalities. Toxicological Sciences 97, 205–213.

Saha, S., New, L.S., Ho, H.K., Chui, W.K., Chan, E.C.Y., 2010. Direct toxicity effects of sulfo-conjugated troglitazone on human hepatocytes. Toxicology Letters 195, 135–141.

Sahi, J., Black, C.B., Hamilton, G.A., Zheng, X., Jolley, S., Rose, K.A., Gilbert, D., LeCluyse, E.L., Sinz, M.W., 2003. Comparative effects of thiazolidinediones on in vitro P450 enzyme induction and inhibition. Drug Metabolism and Disposition: The Biological Fate of Chemicals 31, 439–446.

Schulz-Utermoehl, T., Sarda, S., Foster, J.R., Jacobsen, M., Kenna, J.G., Morikawa, Y., Salmu, J., Gross, G., Wilson, I.D., 2012. Evaluation of the pahrmacokinetics, biotransformation, and hepatic transporter effects of troglitazone in mice with humanized livers. Xenobiotica 42, 503–517.

Tateno, C., Yoshizane, Y., Saito, N., Kataoka, M., Utoh, R., Yamasaki, C., Tachibana, A., Soeno, Y., Asahina, K., Hino, H., Asahara, T., Yokoi, T., Furukawa, T., Yoshizato, K., 2004. Near completely humanized liver in mice shows human-type metabolic responses to drugs. American Journal of Pathology 165, 901–912.

Tettey, J.N., Maggs, J.L., Rapeport, W.G., Pirmohamed, M., Park, B.K., 2001. Enzyme induction dependent bioactivation of troglitazone and troglitazone quinone in vivo. Chemical Research in Toxicology 14, 965–974.

Tietze, F., 1969. Enzymatic method for quantitative determination of nanogram amounts of total and oxidized glutathione: applications to mammalian blood and other tissues. Analytical Biochemistry 27, 502–522.

Tomlinson, E.S., Maggs, J.L., Park, B.K., Back, D.J., 1997. Dexamethasone metabolism in vitro: species differences. Journal of Steroid Biochemistry and Molecular Biology 62, 345–352.

Toyoda, Y., Miyashita, T., Endo, S., Tsuneyama, K., Fukami, T., Nakajima, M., Yokoi, T., 2011. Estradiol and progesterone modulate halothane-induced liver injury in mice. Toxicology Letters 204, 17–24.

Toyoda, Y., Endo, S., Tsuneyama, K., Miyashita, T., Yano, A., Fukami, T., Nakajima, M., Yokoi, T., 2012. Mechanism of exacerbative effect of progesterone on drug-induced liver injury. Toxicological Sciences 126, 16–27.

Usui, T., Hashizume, T., Katumata, T., Yokoi, T., Komuro, S., 2011. In vitro investigation of the glutathione transferase M1 and T1 null genotypes as risk factors for troglitazone-induced liver injury. Drug Metabolism and Disposition: The Biological Fate of Chemicals 39, 1303–1310.

Watanabe, T., Ohashi, Y., Yasuda, M., Takaoka, M., Furukawa, T., Yamoto, T., Sanbuissho, A., Manabe, S., 1999. Was it not possible to predict liver dysfunction caused by troglitazone during the nonclinical safety studies? Reevaluation of Safety 30, 537–546.

Watanabe, T., Furukawa, T., Sharyo, S., Ohashi, Y., Yasuda, M., Takaoka, M., Manabe, S., 2000. Effect of troglitazone on the liver of a Gunn rat model of genetic enzyme polymorphism. Journal of Toxicological Sciences 25, 423–431.

Watanabe, I., Tomita, A., Shimizu, M., Sugawara, M., Yasumo, H., Koishi, R., Takahashi, T., Miyoshi, K., Nakamura, K., Izumi, T., Matusshita, Y., Furukawa, H., Haruyama, H., Koga, T., 2003. A study to survey susceptible genetic factors responsible for troglitazone-associated hepatotoxicity in Japanese patients with type 2 diabetes mellitus. Clinical Pharmacology and Therapeutics 73, 435–455.

Watanabe, T., Sagisaka, H., Arakawa, S., Shibaya, Y., Watanabe, M., Igarashi, I., Tanaka, K., Totsuka, S., Takasaki, W., Manabe, S., 2003. A novel model of continuous depletion of glutathione in mice treated with L-buthionine (S, R)-sulfoximine. Journal of Toxicological Sciences 28, 455–469.

Willey, T.A., Bekos, E.J., Gaver, R.C., Duncan, G.F., Tay, L.K., Beijnen, J.H., Farmen, R.H., 1993. High-performance liquid chromatographic procedure for the quantitative determination of paclitaxel (Taxol) in human plasma. Journal of Chromatography 621, 231–238.

Yamamoto, Y., Yamazaki, H., Ikeda, T., Watanabe, T., Iwabuchi, H., Nakajima, M., Yokoi, T., 2002. Formation of a novel quinone epoxide metabolite of troglitazone with cytotoxicity to HepG2 cells. Drug Metabolism and Disposition: The Biological Fate of Chemicals 30, 155–160.

Yamazaki, H., Shibata, A., Suzuki, M., Nakajima, M., Shimada, N., Guengerich, F.P., Yokoi, T., 1999. Oxidation of troglitazone to a quinone-type metabolite catalyzed by cytochrome P-450 2C8 and P-450 3A4 in human liver microsomes. Drug Metabolism and Disposition: The Biological Fate of Chemicals 27, 1260–1266.

Yang, J., Hao, C., Yang, D., Shi, D., Song, X., Luan, X., Hu, G., Yan, G., 2010. Pregnane X receptor is required for interleukin-6-mediated down-regulation of cytochrome P450 3A4 in human hepatocytes. Toxicology Letters 197, 219–226.

Yoshigae, Y., Konno, K., Takasaki, W., Ikeda, T., 2000. Characterization of UDP-glucuronosyltransferases (UGTs) involved in the metabolism of troglitazone in rats and humans. Journal of Toxicological Sciences 25, 433–441.

Yoshikawa, Y., Morita, M., Hosomi, H., Tsuneyama, K., Fukami, T., Nakajima, M., Yokoi, T., 2009. Knockdown of superoxide dismutase 2 enhances acetaminophen-induced hepatotoxicity in rat. Toxicology 264, 89–95.

1521-009X/12/4012-2267–2272$25.00
DRUG METABOLISM AND DISPOSITION
Copyright © 2012 by The American Society for Pharmacology and Experimental Therapeutics
DMD 40:2267–2272, 2012

Vol. 40, No. 12
47555/3804647

Predictability of Metabolism of Ibuprofen and Naproxen Using Chimeric Mice with Human Hepatocytes

Seigo Sanoh, Aya Horiguchi, Kazumi Sugihara, Yaichiro Kotake, Yoshitaka Tayama, Naoto Uramaru, Hiroki Ohshita, Chise Tateno, Toru Horie, Shigeyuki Kitamura, and Shigeru Ohta

Graduate School of Biomedical and Health Sciences (S.S., A.H., Y.K., S.O.) and Liver Research Project Center (C.T.), Hiroshima University, Hiroshima, Japan; Faculty of Pharmaceutical Science, Hiroshima International University, Hiroshima, Japan (K.S., Y.T.); Nihon Pharmaceutical University, Saitama, Japan (N.U., S.K.); PXB-Mouse Production Department (H.O.) and R&D Department (C.T.), PhoenixBio Co., Ltd., Hiroshima, Japan; and DeThree Research Laboratories, Ibaraki, Japan (T.H.)

Received June 27, 2012; accepted August 30, 2012

ABSTRACT:

Prediction of human drug metabolism is important for drug development. Recently, the number of new drug candidates metabolized by not only cytochrome P450 (P450) but also non-P450 has been increasing. It is necessary to consider species differences in drug metabolism between humans and experimental animals. We examined species differences of drug metabolism, especially between humans and rats, for ibuprofen and (*S*)-naproxen as nonsteroidal anti-inflammatory drugs, which are metabolized by P450 and UDP-glucuronosyltransferase, sulfotransferase, and amino acid *N*-acyltransferase for taurine conjugation in liver, using human chimeric mice (h-PXB mice) repopulated with human hepatocytes and rat chimeric mice (r-PXB mice) transplanted with rat hepatocytes. We performed the direct comparison of excretory metabolites in urine between h-PXB mice and reported data for humans as well as between r-PXB mice and rats after administration of ibuprofen and (*S*)-naproxen. Good agreement for urinary metabolites (percentage of dose) was observed not only between humans and h-PXB mice but also between rats and r-PXB mice. Therefore, the metabolic profiles in humans and rats reflected those in h-PXB mice and r-PXB mice. Our results indicated that h-PXB mice should be helpful for predicting the quantitative metabolic profiles of drugs mediated by P450 and non-P450 in liver, and r-PXB mice should be helpful for evaluation of species differences in these metabolic enzymes.

Introduction

It is important to predict human drug metabolism and pharmacokinetics (PK) during the preclinical stage in the pharmaceutical industry because PK contributes to efficacy and toxicity, and the attrition rate during drug development has been decreasing as a result of improvement of predictability with regard to human metabolism (Kola and Landis, 2004).

The number of new drug candidates metabolized by not only cytochrome P450 (P450) but also non-P450 has been increasing, and they show diverse chemical structures, including a carboxyl group to avoid metabolism by P450. Various approaches to predict human metabolism and PK using an in vitro metabolic system with human liver microsomes, S9 fraction, and hepatocytes have been reported (Obach et al., 1997; Nagilla et al., 2006; Brown et al., 2007; Fagerholm, 2007; Stringer et al., 2008; Anderson et al., 2009; Chiba et al., 2009; Dalvie et al., 2009; Hallifax et al., 2010). However, these methods have some limits for prediction. The above reports indicated that it was difficult to predict secondary metabolism owing to the complication of multiple drug metabolic enzymes such as P450 and non-P450 because the success rate corresponding to the observed metabolites using hepatocytes was low (Anderson et al., 2009; Dalvie et al., 2009).

Chimeric mice with humanized liver, generated using urokinase-type plasminogen activator [uPA(+/+)]/severe combined immunodeficiency (SCID) mice (h-PXB mice) repopulated with human hepatocytes (PhoenixBio Co., Ltd., Hiroshima, Japan) have been reported (Tateno et al., 2004). These mice are transplanted with approximately 80% of human hepatocytes, and the expression levels and activities of P450 and non-P450 in the liver of h-PXB mice are similar to those of humans (Katoh et al., 2004, 2005; Nishimura et al., 2005; Katoh and Yokoi, 2007; Kitamura et al., 2008).

Some specific metabolites were qualitatively detected in the urine and plasma of h-PXB mice (Inoue et al., 2009; Yamazaki et al., 2010; De Serres et al., 2011; Sanoh et al., 2012b). Thus, h-PXB mice could be a good in vivo model for predicting drug metabolism in humans. However, previous investigations for quantitative prediction as well as qualitative prediction of human metabolites involved in multiple metabolic pathways from data in h-PXB mice have been insufficient.

This work was supported by the Japan Society for the Promotion of Science [Grant-in-Aid for Young Scientists (B) 22790109] and PhoenixBio, Co., Ltd.

Article, publication date, and citation information can be found at http://dmd.aspetjournals.org.

http://dx.doi.org/10.1124/dmd.112.047555.

ABBREVIATIONS: PK, pharmacokinetics; P450, cytochrome P450; SCID, severe combined immunodeficiency; h-PXB mice, human chimeric mice; UGT, UDP-glucuronosyltransferase; SULT, sulfotransferase; r-PXB mice, rat chimeric mice; RI, replacement index; LC, liquid chromatography; MS/MS, tandem mass spectrometry.

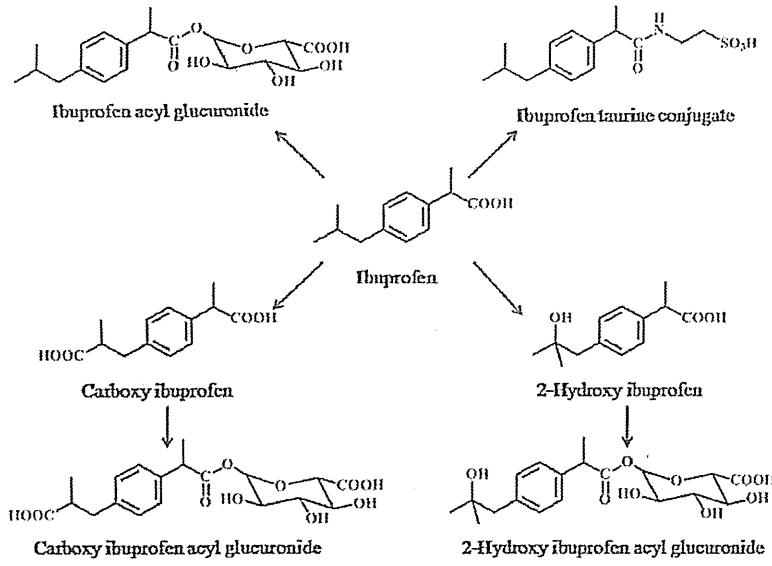

FIG. 1. Proposed metabolic pathways of ibuprofen in humans. This figure was drawn from the data of Shirley et al. (1994) and Kepp et al. (1997).

Racemic ibuprofen and (*S*)-naproxen have been widely used as nonsteroidal anti-inflammatory drugs, which are metabolized by certain metabolic enzymes such as P450 and UDP-glucuronosyltransferase (UGT), sulfotransferase (SULT), and amino acid *N*-acyltransferase for taurine conjugation in liver (Figs. 1 and 2). These metabolites are mainly excreted in urine. Furthermore, species differences in the metabolism of ibuprofen and (*S*)-naproxen between rats and humans have also been reported (Mills et al., 1973; Sugawara et al., 1978).

In this study, rat chimeric mice (r-PXB mice) containing rat hepatocytes were used to compare the metabolism and PK between rats and humans, as well as h-PXB mice, as an in vivo approach (Tateno et al., 2004; Emoto et al., 2005; Yamazaki et al., 2010; Sanoh et al., 2012b). The aim of this study was to assess the quantitative predictability of the metabolism by P450 and non-P450 by examining urinary excreted metabolites in h-PXB mice and r-PXB mice after administration of ibuprofen and (*S*)-naproxen.

Materials and Methods

Chemicals. 2-(4-Isobutylphenyl)-propionic acid (ibuprofen) and 2-(3-benzoylphenyl)-propionic acid (ketoprofen) were purchased from Wako Pure Chemicals (Osaka, Japan). (*S*)-(+)-2-(6-Methoxy-2-naphthyl)propionic acid [(*S*)-naproxen] was purchased from Cayman Chemical (Ann Arbor, Michigan). 2-[4-(2-Carboxypropyl)phenyl]-propionic acid (carboxy ibuprofen), 2-[4-(2-hydroxy-2-methylpropyl) phenyl]-propionic acid (2-hydroxylibuprofen), (*S*)-(+)-2-(6-hydroxy-2-naphthyl)-propionic acid [(*S*)-*O*-desmethylnaproxen], and (*S*)-naproxen acyl-β-D-glucuronide were obtained from Toronto Research Chemicals, Inc. (North York, ON, Canada). Ibuprofen taurine conjugate was synthesized in accordance with Shirley et al. (1994). All of the other reagents and solvents were commercial products of the highest available grade or analytical grade.

Animals. The present study was approved by the animal ethics committee and was conducted in accordance with the regulations on the use of living modified organisms of Hiroshima University. Sprague-Dawley rats (6 weeks of age) and SCID mice (10 weeks of age) were purchased from Charles River Laboratories Japan, Inc. (Yokohama, Japan). h-PXB mice and r-PXB mice (10 weeks of age), transplanted with human and rat hepatocytes, respectively, were prepared by PhoenixBio Co., Ltd. (Hiroshima, Japan). All animals were housed in a temperature- and humidity-controlled environment under a 12-h light/dark cycle with free access to tap water and food.

Human hepatocytes of a donor (African-American boy, 5 years old) were obtained from BD Biosciences (San Jose, CA). Rat hepatocytes for the preparation of r-PXB mice were isolated from the liver of Sprague-Dawley rats (4

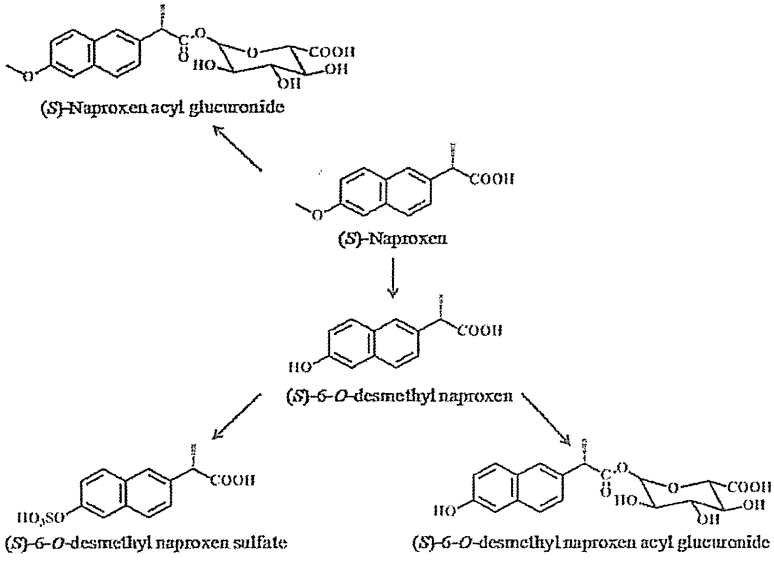

FIG. 2. Proposed metabolic pathways of (*S*)-naproxen in humans. This figure was drawn from the data of Sugawara et al. (1978).

weeks of age, male). The replacement ratio of host hepatocytes with human or rat hepatocytes, calculated as the replacement index (RI), was determined by measurement of the level of human or rat albumin in blood collected from the tail vein of each PXB mouse (Tateno et al., 2004; Emoto et al., 2005). Average RI values of h-PXB mice and r-PXB mice used in this study were 78 and nearly 100%, respectively.

Administration of Ibuprofen and (*S*)-Naproxen. Ibuprofen and (*S*)-naproxen solution (5 ml/kg) were administered orally to each animal at 20 and *10 mg/kg b.wt., respectively*, which included 0.5% carboxymethylcellulose with a requisite minimum amount of potassium hydroxide for solution. After treatment of ibuprofen and (*S*)-naproxen, pooled urine samples were collected until 24 and 48 h, respectively.

Analysis and Quantitation of Ibuprofen, (*S*)-Naproxen, and Their Metabolites. *Ibuprofen.* Pooled urine (20 μl) was mixed with 0.1% formic acid (500 μl) and internal standard solution (30 μg/ml ketoprofen, 10 μl). These mixtures were absorbed to a MonoSpin C18 column (GL Sciences Inc., Tokyo, Japan) for solid-phase extraction. Samples purified by elution with 50% acetonitrile were subjected to liquid chromatography (LC)-tandem mass spectrometry (MS/MS). The concentrations of ibuprofen acyl glucuronide, carboxy ibuprofen acyl glucuronide and 2-hydroxyibuprofen acyl glucuronide were determined as increased amounts of ibuprofen, carboxy ibuprofen, and 2-hydroxyibuprofen by hydrolysis using 1 M sodium hydroxide before solid-phase extraction.

(S)-Naproxen. Pooled urine (20 μl) was mixed with acetonitrile (30 μl). After centrifugation, the supernatants with 10 mM ammonium acetate were subjected to LC-MS/MS.

The concentrations of (*S*)-6-*O*-desmethyl naproxen glucuronide were determined as increased amounts of 6-*O*-desmethyl naproxen by incubation for 2 h at 37°C using β-glucuronidase (20 μl) in 1 M acetate buffer (100 μl) after the hepatocytes were thawed. The concentration of 6-*O*-desmethyl naproxen sulfate was estimated by subtracting the concentration of 6-*O*-desmethyl naproxen glucuronide from that of total hydrolyzed 6-*O*-desmethyl naproxen after enzyme deconjugation for 2 h at 37°C using β-glucuronidase-arylsulfatase (20 μl) in 1 M acetate buffer. Incubation mixtures were extracted with ethyl acetate (5 ml) and internal standard solution (ketoprofen). The organic layer (4 ml) was evaporated to dryness, and the residues were dissolved in aqueous acetonitrile (100 μl). Aliquots of 10 μl were applied to the LC-MS/MS system.

LC-MS/MS conditions. Aliquots (10 μl) of urine samples were introduced into the LC system (Agilent Technologies, Santa Clara, CA). The mobile phase condition for ibuprofen and (*S*)-naproxen consisted of 10 mM ammonium acetate (A) and acetonitrile (B) through an Inersil ODS-3 column (5 μl, 50 × 2.1 mm; GL Sciences Inc.) at 40°C. The flow rate was set at 0.2 ml/min. The starting condition for the LC gradient was 90:10 (A/B). From 0 to 5 min, the mobile phase composition was changed to 10:90 (A/B), and this was maintained until 8 min. The gradient was then returned to 90:10 (A/B) linearly from 8 to 8.1 min, and the column was reequilibrated to the initial condition from 8.1 to 15 min. The elution times of ibuprofen, ibuprofen taurine conjugate, carboxy ibuprofen, 2-hydroxyibuprofen, (*S*)-naproxen, naproxen acyl glucuronide, (*S*)-6-*O*-desmethylnaproxen, and ketoprofen as internal standard were 5.9, 5.8, 0.9, 4.2, 5.0, 4.9, 4.0, and 5.0 min, respectively.

The MS/MS experiments were conducted by using API2000 LC-MS/MS systems (Applied Biosystems, Foster, CA). Mass numbers of the ionization mode, molecular ion, and product ion for ibuprofen, (*S*)-naproxen, and their metabolites were as follows: ibuprofen m/z = 204.9 $[M - H]^-$ to 158.5, ibuprofen taurine conjugate m/z = 311.9 $[M - H]^-$ to 123.4, carboxy ibuprofen m/z = 235.1 $[M - H]^-$ to 72.6, 2-hydroxyibuprofen m/z = 221.3 $[M - H]^-$ to 176.9, (*S*)-naproxen m/z = 228.7 $[M - H]^-$ to 168.5, naproxen acyl glucuronide m/z = 404.8 $[M - H]^-$ to 169.1, (*S*)-6-*O*-desmethylnaproxen m/z = 214.7 $[M - H]^-$ to 170.4, and ketoprofen m/z = 253.2 $[M - H]^-$ to 208.7.

Results

Predictability of Metabolic Profiles of Ibuprofen in Humans. Proposed metabolic pathways of ibuprofen were reported previously from the urinary metabolic profile excreted in humans after oral administration of ibuprofen (Fig. 1). Six metabolites, ibuprofen acyl glucuronide, ibuprofen taurine conjugate, carboxy ibuprofen, carboxy ibuprofen glucuronide, 2-hydroxyibuprofen, and 2-hydroxyibuprofen acyl glucuronide were predominantly detected in urine (Shirley et al., 1994; Kepp et al., 1997). The percentage values in Table 1 indicate urinary excreted metabolites in relation to the dose (percentage of dose) after oral administration of ibuprofen in humans (400 and 600 mg/person), h-PXB mice (20 mg/kg), rats (20 mg/kg), and r-PXB mice (20 mg/kg). These metabolites observed in humans were also identified in h-PXB mice, rats, and r-PXB mice. The amount of excreted unchanged form of ibuprofen in urine was negligible in all animals in this study (less than 2% of the dose). Amounts of excreted acyl glucuronide conjugates in human urine were higher than those of rats, whereas the amount of 2-hydroxyibuprofen in humans was lower than that of rats. We directly compared six urinary metabolites (percentage of dose) between humans and rats (Fig. 3A). There were weak correlations (r^2 = 0.471, p = 0.132). The correlations reflect species differences in the excretory metabolic profile between humans and rats. To investigate whether these differences reflect each chimeric mice, we directly compared the excreted metabolites between humans and h-PXB mice. This result showed good correlation (r^2 = 0.863, p = 0.007) (Fig. 3B). In addition, good correlation was also found between rats and r-PXB mice (r^2 = 0.928, p = 0.002) (Fig. 3C), whereas the relationship between h-PXB mice and r-PXB mice was weaker (r^2 = 0.286, p = 0.274) (Fig. 3D). These data suggested that the excretory metabolic profiles in humans and rats qualitatively reflected those of h-PXB mice and r-PXB mice, respectively. In a comparison with SCID mice, the host of chimeric mice, a low correlation was observed between humans and SCID mice (r^2 = 0.246, p = 0.317) and between h-PXB mice and SCID mice (r^2 = 0.129, p = 0.484) (Fig. 3, E and F).

Predictability of Metabolic Profiles of (*S*)-Naproxen in Humans. (*S*)-Naproxen is metabolized into four metabolites: (*S*)-naproxen acyl glucuronide, (*S*)-6-*O*-desmethylnaproxen, and the latter's metabolites, (*S*)-6-*O*-desmethylnaproxen sulfate and (*S*)-6-*O*-desmethylnaproxen

TABLE 1

Cumulative urinary excretion of six metabolites of ibuprofen

Human data (mean ± S.D., n = 4) after oral administration of ibuprofen (600 mg/person) are from Kepp et al. (1997). Data on the amount of ibuprofen taurine conjugate (mean ± S.E., n = 4) in humans after oral administration (400 mg/person) are from Shirley et al. (1994). Each value for h-PXB mice, r-PXB mice, rats, and SCID mice after oral administration (20 mg/kg) is the mean ± S.D. of n = 8, 3, 3, and 3 respectively.

Species	Urinary Excreted Metabolites					
	Ibuprofen Acyl Glucuronide	Ibuprofen Taurine Conjugate	Carboxy Ibuprofen	Carboxy Ibuprofen Glucuronide	2-Hydroxyibuprofen	2-Hydroxyibuprofen Acyl Glucuronide
			% dose			
h-PXB mice	11.3 ± 8.5	0.4 ± 0.4	5.4 ± 2.3	7.0 ± 3.4	2.4 ± 2.3	8.4 ± 4.7
Humans	11.6 ± 7.6	1.5 ± 0.5	13.5 ± 3.7	11.6 ± 7.3	5.9 ± 2.7	28.1 ± 8.5
r-PXB mice	0.9 ± 0.7	0.2 ± 0.2	4.4 ± 3.5	1.2 ± 1.1	8.8 ± 6.9	23.8 ± 17.4
Rats	0.2 ± 0.1	$8.0 \times 10^{-3} \pm 2.0 \times 10^{-3}$	2.9 ± 0.5	0.8 ± 0.6	34.5 ± 9.8	19.8 ± 2.4
SCID mice	2.5 ± 1.7	0.5 ± 0.3	5.3 ± 2.5	0.2 ± 4.3	1.5 ± 0.6	5.3 ± 2.8

acyl glucuronide, which were reported to be mainly excreted in the urine of humans (Fig. 2) (Sugawara et al., 1978). (*S*)-Naproxen was also excreted at negligible levels. Table 2 shows the percentage of each urinary metabolite after oral administration of (*S*)-naproxen in humans (200 mg/person), h-PXB mice (10 mg/kg), rats (10 mg/kg), and r-PXB mice (10 mg/kg). Four metabolites reported in humans were also found in the urine of h-PXB mice, rats, and r-PXB mice. Amounts of excreted naproxen acyl glucuronide and 6-*O*-desmethylnaproxen acyl glucuronide in human urine were higher than those of rats, whereas the amounts of 6-*O*-desmethylnaproxen and its sulfate in human were lower than that of rats.

We compared the percentages of dose of these excretory metabolites with those of chimeric mice. The amounts of naproxen acyl glucuronide, which was mainly observed in human urine and that of 6-desmethylnaproxen, the amount of which was low, corresponded to those of h-PXB mice. On the other hand, the amount of 6-*O*-desmethylnaproxen sulfate, which was mainly observed in rats, and that of naproxen acyl glucuronide, which was lower, were in close agreement with those of r-PXB mice. Differences in excretory metabolic profiles between humans and rats were similar to those between h-PXB mice and r-PXB mice.

Discussion

Identification of primary metabolites contributes to drug design for stable metabolic analogs. Not only primary metabolites but also secondary metabolites could be involved in efficacy and toxicity via biotransformation.

It is also necessary to reflect on species differences in isoform composition, expression, and activity of drug metabolic enzymes between humans and experimental animals (Martignoni et al., 2006). We considered that h-PXB mice with a high replacement of human hepatocytes may be useful for prediction of human metabolism because the expression levels and activities of both P450 and non-P450 enzymes reflect those of the donor hepatocytes (Yoshitsugu et al., 2006; Yamasaki et al., 2010). Sanoh et al. (2012a) demonstrated the predictability of human PK of 13 model compounds, including ibuprofen and (*S*)-naproxen, metabolized by P450 and non-P450, using h-PXB mice. For ibuprofen, the predictability of in vivo intrinsic clearance in h-PXB mice reflected that observed in humans (Sanoh et al., 2012a).

Ibuprofen was metabolized by CYP2C9 and UGT2B7 (Hamman et al., 1997; Buchheit et al., 2011). In addition, a taurine conjugate of ibuprofen was identified in the urine of humans as a minor metabolite (Shirley et al., 1994). (*S*)-Naproxen was metabolized by CYP2C9, CYP1A2, UGT2B7, and SULT1A1 (Rodrigues et al., 1996; Bowalgaha et al., 2005; Falany et al., 2005).

TABLE 2

Cumulative urinary excretion of four metabolites of (S)-naproxen

Human data (mean ± S.D., $n = 3$) after oral administration (200 mg/person) are from Sugawara et al. (1978). The amounts of acyl glucuronide formed were determined by hydrolysis with β-glucuronidase. The amount of sulfate of desmethyl naproxen was determined by hydrolysis with 2 N HCl (Sugawara et al., 1978). Data on metabolites of h-PXB mice, r-PXB mice, and rats after oral administration (10 mg/kg) are means ± S.D. of $n = 3$.

Species	Urinary Excreted Metabolites			
	(*S*)-Naproxen Acyl Glucuronide	(*S*)-6-*O*-Desmethyl Naproxen	(*S*)-6-*O*-Desmethyl Naproxen Acyl Glucuronide	(*S*)-6-*O*-Desmethylnaproxen Sulfate
	% dose			
h-PXB mice	26.5 ± 6.6	0.2 ± 0.2	1.0 ± 0.6	12.4 ± 3.1
Humans	25.3 ± 6.7	0.9 ± 0.2	8.3 ± 2.0	10.8 ± 0.5
r-PXB mice	2.9 ± 2.9	2.5 ± 1.4	0.5 ± 0.5	57.3 ± 6.1
Rats	1.2 ± 0.7	5.3 ± 3.8	1.8 ± 0.4	56.9 ± 8.7

CYP2C9 is one of the most abundant P450 enzymes in human liver. CYP2C9 metabolizes approximately 20% of clinical drugs, including a number of drugs with a narrow therapeutic ranges. UGT2B7 also contributes to the metabolism of numerous clinical drugs (Williams et al., 2004).

Ibuprofen and (*S*)-naproxen are suitable as representative model compounds to elucidate the predictability of multiple metabolic pathways associated with P450 and non-P450 using h-PXB mice. Metabolites of ibuprofen and (*S*)-naproxen were reported to be excreted in urine, which suggested that the kidneys are the main excretion route (Sugawara et al., 1978; Shirley et al., 1994; Kepp et al., 1997). Furthermore, we used r-PXB mice as a control model in consideration of species differences between humans and rats in this study.

Six metabolites of ibuprofen, which were identified in humans, were also found in the urine of h-PXB mice, r-PXB mice, and rats. On the other hand, fecal excretion of these metabolites was low (data not shown). These findings suggested that h-PXB mice reflected species differences of the main excretory pathways of cefmetazole (Okumura et al., 2007). We could confirm species differences in the amounts of urinary excretion of these metabolites between humans and rats because a weak correlation ($r^2 = 0.471$, $p = 0.132$) was observed, as shown in Fig. 3A. There were good correlations between humans and h-PXB mice ($r^2 = 0.863$, $p = 0.007$), as well as between rats and r-PXB mice ($r^2 = 0.928$, $p = 0.002$) (Fig. 3, B and C). Therefore, species differences in urinary excretion of metabolites between humans and rats reflect the relationship between h-PXB mice and r-PXB mice.

(*S*)-Naproxen is metabolized in humans by acyl glucuronidation, O-demethylation, and further sulfation and glucuronidation. Four metabolites were found in urine after administration in h-PXB mice, r-PXB mice, and rats. Species differences in excretory metabolites between humans and rats reflect the levels in humans and rats because amounts of each urinary metabolite were similar between humans and h-PXB mice as well as rats and r-PXB mice, in common with the results for ibuprofen.

We used h-PXB mice for which the average RI values were approximately 80%. The contribution of the remaining 20% of host hepatocytes may have influenced the predictability. Direct comparison of excretory metabolites between humans and SCID mice as host mice gave a value of $r^2 = 0.246$ ($p = 0.317$) (Fig. 3E). In addition, there was no correlation ($r^2 = 0.129$, $p = 0.484$) between h-PXB mice and SCID mice (Fig. 3F), although in vitro intrinsic clearance of ibuprofen in SCID mouse hepatocytes was similar to that of h-PXB mouse hepatocytes (Sanoh et al., 2012a). This result suggested that the remaining host mouse hepatocytes did not affect the predictability using h-PXB mice despite species differences between humans and SCID mice being observed. For r-PXB mice, it is not necessary to consider the remaining host mouse hepatocytes because RI of rat hepatocytes in liver of r-PXB mice is approximately 100%.

In this study, analysis of the predictability using h-PXB mice and r-PXB mice was conducted by oral administration. It is also necessary to consider the effects of the intestine, which is not humanized in h-PXB mice, in cases of oral administration. We compared recovery metabolites in h-PXB mice after intravenous and oral administration of ibuprofen. Because these results showed good correlation ($r^2 = 0.900$, $p = 0.004$), metabolic activities of ibuprofen in mouse intestine may be negligible (data not shown).

Our results using ibuprofen and (*S*)-naproxen indicated that in vivo metabolic activities of P450 and non-P450, such as those involving UGT, SULT, and amino acid *N*-acyltransferase in h-PXB mice and r-PXB mice, should be similar to those of humans and rats. In this study, r-PXB mice were used as the control animal for transplantation